Journal of the Mechanics and Physics of Solids 125 (2019) 1–21

Contents lists available at ScienceDirect

Journal of the Mechanics and Physics of Solids

journal homepage: www.elsevier.com/locate/jmps

Mechanics of electrophoresis-induced reversible hydrogel adhesion

An Xin, Runrun Zhang, Kunhao Yu, Qiming Wang*

Sonny Astani Department of Civil and Environmental Engineering, University of Southern California, Los Angeles, CA 90089, United States

ARTICLE INFO

Article history:
Received 1 October 2018
Revised 10 December 2018
Accepted 10 December 2018
Available online 11 December 2018

Keywords:
Reversible adhesion
Electrophoresis
Dynamic bond
Interpenetrating network model
Diffusion-reaction model

ABSTRACT

Adhesion of soft materials is a double-edged sword that can induce both advantages and disadvantages. On-demand control of the adhesion of soft materials with external stimuli is naturally desirable. Electrophoresis-induced hydrogel adhesion is such a technology that induces electrically-triggered reversible adhesion and may be useful for various engineering applications. Despite the potential, the detailed mechanism is still elusive. Here, we establish an analytical theory framework to model the electrophoresis-induced reversible adhesion. We consider that during the electrophoresis process, free charged chains are driven by the electric field to move across the interface to interpenetrate into the respective material matrix, and form weak ionic bonds with chains with opposite charges. We model the interpenetration of the charged polymer chains as an electrically-driven diffusion-reaction process. The chain diffusion follows an electrically-driven reptation-like motion, and cationic-anionic bond formation follows a bell-like chemical reaction. We predict that the electrophoresis-induced adhesion increases with the electrophoresis time and reaches a plateau as the electrophoresis process is long enough. We theoretically study the effects of the electric force, the polymer chain length, and the chain friction coefficient on the hydrogel adhesion. We also predict that under reverse electrophoresis the hydrogel adhesion decreases with the process time. Our theoretical results agree well with the experiments for both electrophoresis-induced adhesion and adhesion releasing. We expect our theoretical model may facilitate the quantitative understanding and optimization of various methods for actively controlling the adhesion of soft materials.

1. Introduction

The tough adhesions between similar or dissimilar soft materials can facilitate a number of applications, such as flexible electronics (Keplinger et al., 2013; Kim et al., 2016; Larson et al., 2016; Sun et al., 2014; Wirthl et al., 2017; Yang et al., 2015), soft actuators (Acome et al., 2018; Keplinger et al., 2013; Robinson et al., 2015; Yang et al., 2016), energy generators (Lee et al., 2018; Pu et al., 2017), biomedical dressing (Li et al., 2017), and advanced manufacturing (Liu et al., 2018; Yuk et al., 2015; Yuk et al., 2016). At the same time, the adhesion between soft materials may also induce unnecessary inconvenience, such as failures during the disassembly of soft material laminates (Ghatak and Chaudhury, 2003; Ghatak et al., 2000; Sarkar et al., 2005; Sarkar et al., 2004; Shull et al., 2000). It is naturally desirable to develop paradigms to on-demand control the adhesion between soft materials: high adhesion when an external control is applied, and low adhesion when the control is

* Corresponding author.
E-mail address: qimingw@usc.edu (Q. Wang).

https://doi.org/10.1016/j.jmps.2018.12.007
0022-5096/

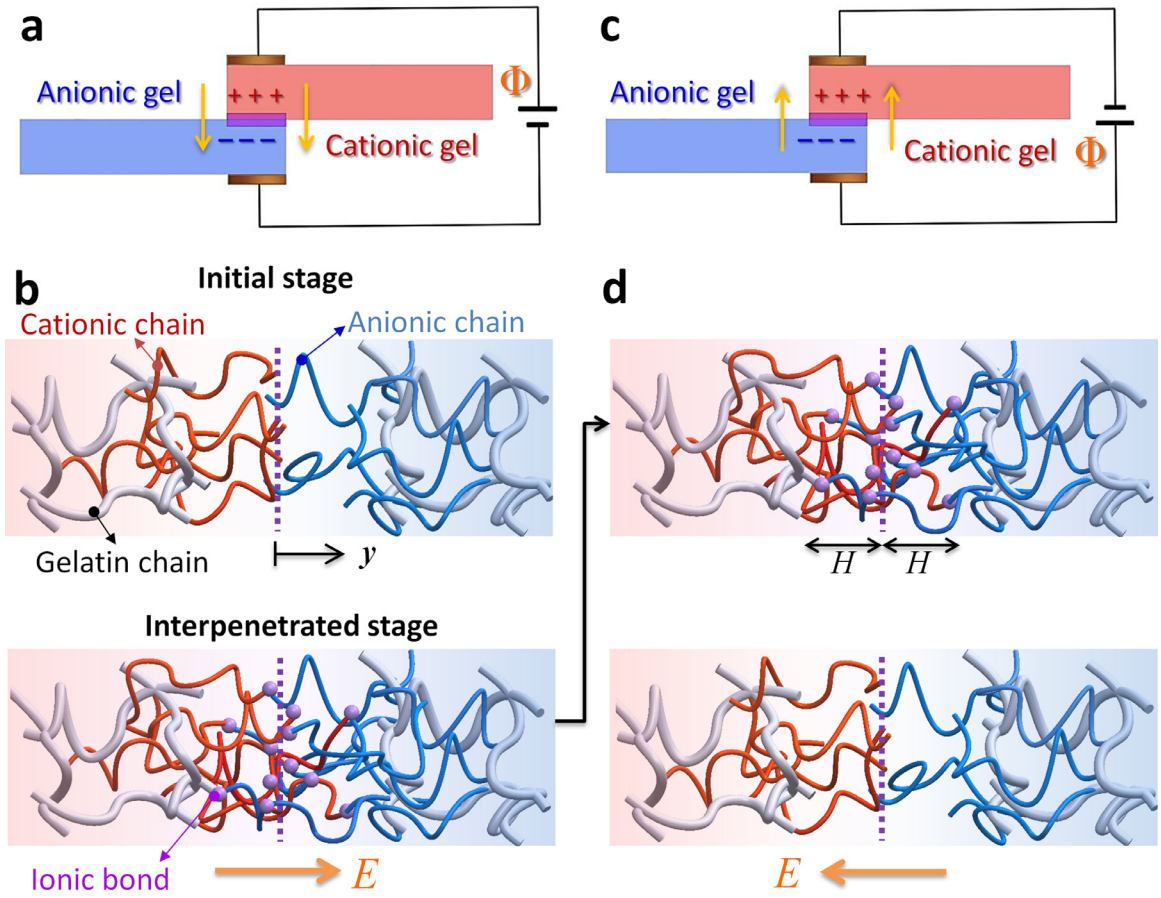

Fig. 1. Schematics for (ab) electrophoresis-induced hydrogel adhesion and (cd) reverse electric-field-induced adhesion releasing. (b) and (d) are the zoomed-in interpenetration regions shown in (a) and (c), respectively.

released or another external control is triggered. However, most of the existing strategies are primarily focused on adhesion promotion, and few on on-demand switching the adhesion on-off (Kim et al., 2010; Zhao et al., 2017).

Electrophoresis enabled adhesion between charged hydrogels is such a method that can be used to on-demand control the hydrogel adhesion through external electric fields. (Asoh, 2016; Asoh et al., 2012, 2013; Asoh and Kikuchi, 2010, 2012; Asoh et al., 2015). Specifically, a positively-charged cationic hydrogel is laminated with a negatively-charged anionic hydrogel with the bonding segment under an electric field (Fig. 1a). Within the bonding segment, the cationic chains are driven by the electric field to penetrate into the hydrogel matrix with the anionic chains, and then form ionic bonds with the anionic chains (Fig. 1b). Likewise, the anionic chains also penetrate into the cationic hydrogel matrix to form ionic bonds with cationic chains. This chain interpenetration can enable relatively strong hydrogel adhesion. When an electric field with the reverse direction is applied, the formed ionic bonds will be gradually dissociated, and cationic (anionic) chains diffuse out of the anionic (cationic) hydrogel matrix; thus, the formed adhesion will be released (Fig. 1cd). Such control is simple and elegant because the only requirement is a remotely controlled electric field. This method may find broad applications where tough adhesion and weak adhesion are alternatively required, such as robot locomotion and flying (Graule et al., 2016), reversible under-water adhesives (Zhao et al., 2017), reversible biomedical dressing (Li et al., 2017), and reversible advanced manufacturing and assembly (Asoh, 2016). Despite the potential, the detailed mechanism has not been well understood. For example, it is unknown how to model the interpenetration behavior of charged polymer chains under the external electric field. It is also elusive how to link the interfacial polymer chain behavior to the interfacial bonding strength within the framework of charged hydrogels.

Here, we establish an analytical theory framework for the electrophoresis enabled reversible adhesion. We model the interpenetration of the charged polymer chains as an electrically-driven diffusion-reaction process. The chain diffusion follows an electrically-driven reptation-like motion, and cationic-anionic bond formation follows a bell-like chemical reaction. We predict that the electrophoresis-induced hydrogel adhesion increases with the electrophoresis time and reaches a plateau as the electrophoresis process is long enough. We theoretically study the effects of the electric force, the polymer chain length, and the chain friction coefficient on the hydrogel adhesion. We also predict that the hydrogel adhesion decreases

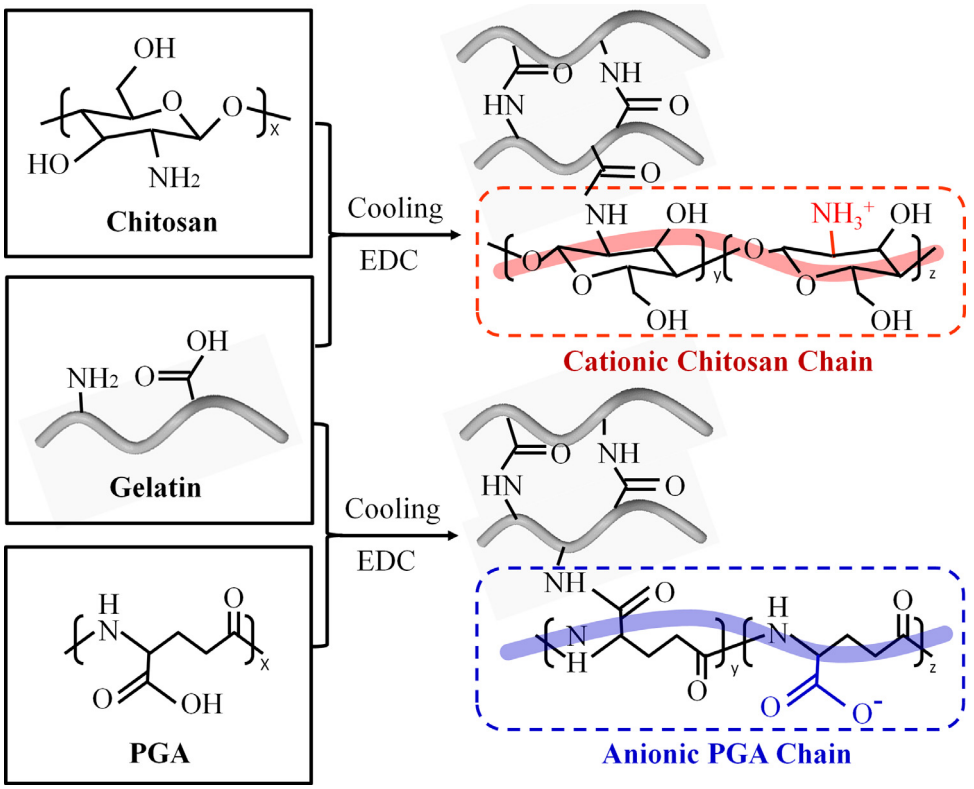

Fig. 2. Chemical structures for the cationic Chitosan hydrogel and anionic PGA hydrogel. These two hydrogels are made based on a neutral Gelatin hydrogel that was incorporated with cationic and anionic ions, respectively.

with the process time under the reverse electrophoresis. Our theoretical results agree well with the experiments for both electrophoresis-induced hydrogel adhesion and adhesion releasing. We expect our theoretical model may facilitate the quantitative understanding and optimization of various methods for the reversible adhesion of soft materials.

The plan of the paper is as follows: Section 2 introduces the experimental procedures of the electrophoresis-induced hydrogel adhesion and adhesion releasing. Section 3 first presents a model for the covalently crosslinked parent hydrogels, and then a theoretical framework to consider the electrically-driven interpenetration of the polymer chains. Subsequently, a theory is presented to model the interfacial strength of the bonded interface. Based on the electrophoresis-induced hydrogel adhesion, a theory is accordingly developed to model the adhesion releasing under the reverse electrophoresis. Based on the theoretical framework, in Section 4 we analytically elucidate the stress-strain behaviors of electrophoresis-treated hydrogel laminates and their adhesion strengths in a function of the electrophoresis time. We then systematically examine the effects of electric force, chain length distribution, and Rouse friction coefficient on the adhesion strength of the hydrogel laminates. We then predict the electrophoresis-induced reduced adhesion in a function of reverse electrophoresis time. Subsequently, in Section 5, the theoretical results are quantitatively compared with experimentally measured results. The conclusive remarks will be given in Section 6.

2. Experimental

Gelatin aqueous solution (10 wt%) was obtained by stirring and heating on a CORNING platform for 15 min at 45 °C (Fig. 2). poly-L-γ-glutamate acid sodium salt (PGA, 10 wt% of the gelatin) and Chitosan (10 wt% of the gelatin) were dissolved into gelatin aqueous solution respectively while stirring and heating continued for another 15 min at 45 °C. Both two aqueous solutions were then injected into glass plates molds with $15 \times 5 \times 1.5$ mm spacing and cured through chemically cross-linking gelatin at 4 °C for over 1 h. 0.3834 g N-(3-Dimethylaminopropyl)-N'-ethylcarbodiimide hydrochloride (EDC) were dissolved into 200 mL DI water as the dispersion medium. The cured Chitosan and PGA gels were immersed into the EDC aqueous solution for 30 min to obtain the hydrogel samples. Note that all chemicals were commercially available without further purification. Gelatin (Type A) from porcine skin, poly-L-γ-glutamate acid sodium salt (PGA), chitosan, and N-(3-Dimethylaminopropyl)-N'-ethylcarbodiimide hydrochloride (EDC) were all purchased from Sigma-Aldrich, USA.

The electrophoresis experiment was carried out between two copper electrodes. PGA and Chitosan hydrogels were held in contact between the copper electrodes, with the PGA hydrogel on the cathode and the Chitosan hydrogel on the anode. The contact area is around 1 mm × 7 mm, measured in specific experiments. A controllable voltage source was used to create

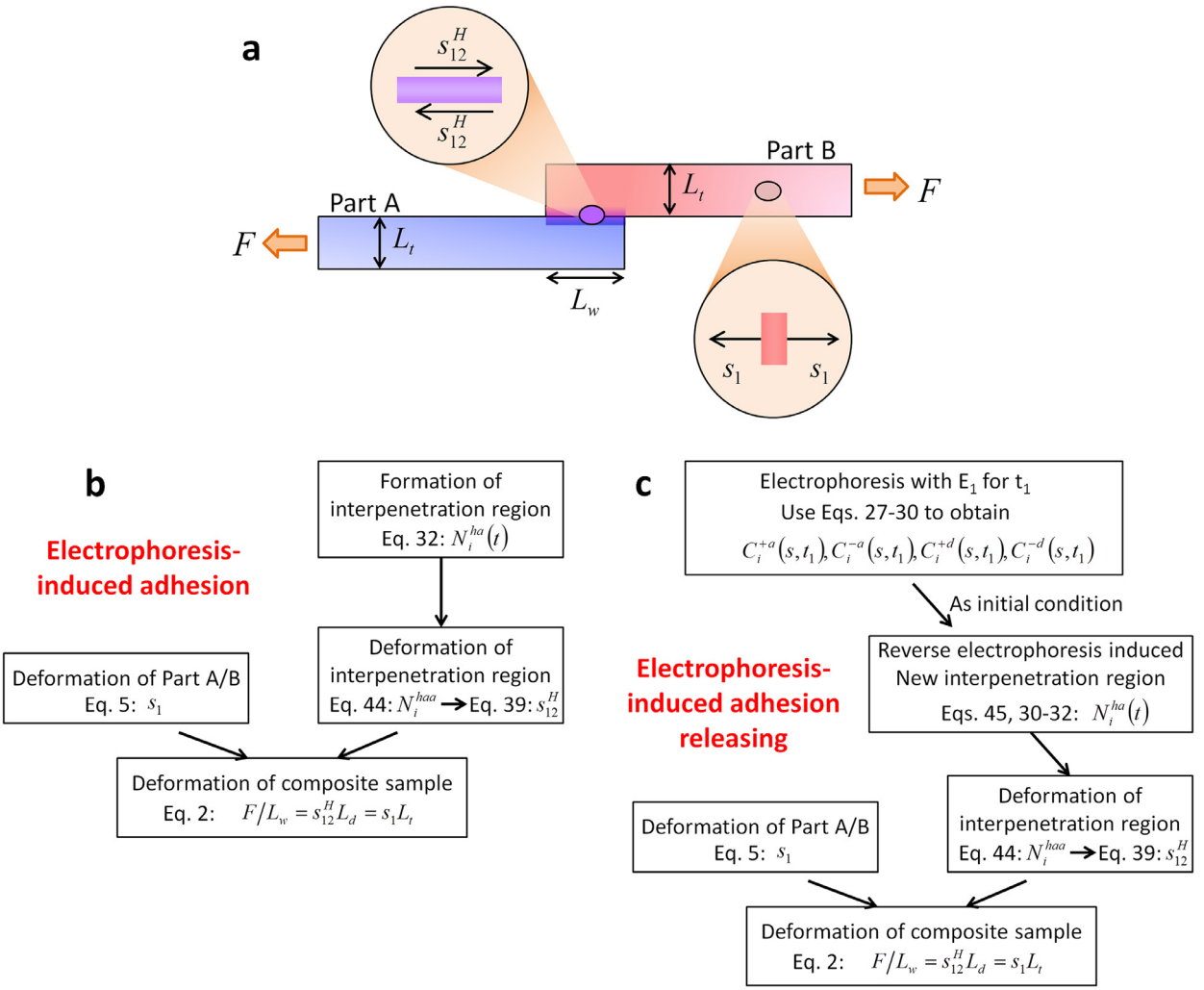

Fig. 3. (a) A schematic to show the stress-state in the material bulk and around the interpenetration region during a shear-lag test. Flow charts to show the calculation process of the electrophoresis-induced (b) adhesion and (c) adhesion releasing, respectively.

various electric fields. To detach the adhered hydrogels, an inverse electric field was applied on the contacted hydrogels. A stopwatch was used to record the electrophoresis time. Note that the time of our electrophoresis experiment is relatively short (within 60 s), and we did not observe bubble formation that is expected in the water electrolysis experiment. Therefore, we neglect the effect of water electrolysis in the following study. Instron 5942 was used to test the adhesive strength between the PGA and Chitosan hydrogels with a small loading rate 0.01 s^{-1}. The adhesive strength is considered as the lap shear adhesion strength.

3. The analytical model

Two hydrogels with charges of opposite signs are taken to make contact within a small area (Figs. 1ab and 3a). The cationic hydrogel is denoted as part A, and the anionic hydrogel as part B. An electric field is applied across the thickness for a period of time t. Driven by the electric field, the cationic chains in part A will penetrate into part B, and the anionic chains in part B will penetrate into part A. The penetrated chains will form ionic bonds with the oppositely-charged chains. After the application of the electric field, an interpenetration region forms around the contact interface. Therefore, a composite sample is formed with three segments: part A, interpenetration region, and part B. The deformation of the composite sample will be considered in Section 3.1. The modeling of constitutive behaviors of part A and B will be presented in Section 3.2. The modeling of the interpenetration region will be given in Sections 3.3 and 3.4. Flow charts of the theoretical calculation processes are shown in Fig. 3bc.

The bonding of two similar hydrogel materials with opposite charges is considered. Initially, two pieces of identical gels (Gelatin) are fabricated, and PGA and Chitosan are added to gels to make them cationic and anionic, respectively (Fig. 2).

Therefore, there are crosslinked and uncrosslinked chains within the matrix of two hydrogels. The crosslinked chains (i.e., Gelatin) are bridged by covalent bonds. The uncrosslinked chains are charged over the whole chain, and one end of the chain is linked to the backbone of the crosslinked chains (Fig. 2). We assume that the uncrosslinked chains do not contribute to the strain energy of the hydrogel matrix. We expect that within a certain strain range, two hydrogel samples are assumed to have the same stress-strain behavior; this point can be validated by the experimental data in Fig. 12a. The uncrosslinked charged chains are mobile within the hydrogel matrix. Once these charged chains penetrate into the hydrogel matrix with charged chains with opposite charges, ionic bonds will form to bridge chains, thus forming the interfacial bonding.

In this section, we will first introduce the deformation of the shear-lag sample. Then, we will introduce a polymer network model for the hydrogel with a covalent polymer network. Subsequently, we will present a model to explain the electric field assisted chain penetration across the interface. Along with the reaction term, we derive the model for the electrophoresis enabled adhesion of the hydrogel. Finally, with an electric field with a reverse direction, a model for the electrophoresis enabled adhesion releasing will be constructed.

3.1. Deformation of the shear-lag sample

We consider a shear-lag test shown in Fig. 3a. We assume the thickness of the hydrogel is L_t, the depth normal to the paper is L_d, and the contact width is L_w. Under tensile deformation, the uniaxial stretch in part A and part B is λ and shear stretch of the interpenetration region is λ^H. The size of the interpenetration region is much smaller than those of part A and part B; therefore, the stretch of the whole sample should be approximated as λ. According to the force balance between the interpenetration region and the part A/B, the uniaxial force is

$$F = s_{12}^H L_w L_d = s_1 L_w L_t \tag{1}$$

where s_1 is the uniaxial nominal stress of the part A/B (given by Eq. (5) in Section 3.2) and s_{12}^H is the shear stress of the interpenetration region (given by Eq. (39) in Section 3.4.3). Eq. (1) can be rewritten as

$$\frac{F}{L_w} = s_{12}^H L_d = s_1 L_t \tag{2}$$

Eq. (39) will be used in the discussion in Sections 4 and 5. The quantity with a dimension N/m is the shared quantity between the shear region and uniaxial region.

3.2. Modeling covalent polymer networks

We model Part A/B as covalent polymer networks using the Arruda–Boyce model (Arruda and Boyce, 1993). The Arruda–Boyce model assumes that the polymer chains feature the same length and self-organize into body-centered eight-chain structures. The free energy density function of the deformed network is written as

$$W_0 = W_{mix} + N_0 n_0 k_B T \left(\frac{\beta}{\tanh \beta} + \ln \frac{\beta}{\sinh \beta} \right) \tag{3}$$

where k_B is the Boltzmann constant, T is the temperature in Kelvin, n_0 is the average Kuhn segment number of the chain, N_0 is the chain number per unit volume of material, $\beta = L^{-1}(\Lambda/\sqrt{n_0})$, $L^{-1}()$ is the inverse Langevin function, and Λ is the chain stretch. W_{mix} is the mixing free energy to characterize the interaction between the polymer chains and the solvent water. Considering the short experiment time that is much shorter than the time scale of water diffusion within the sample, we consider W_{mix} as a constant in this problem.

To link the chain stretch to the macroscopic deformation, it follows an affined deformation model (Arruda and Boyce, 1993; Rubinstein and Colby, 2003; Treloar, 1975), so that under the material deformation with a deformation gradient $\mathbf{F}$ the stretch of the chain is

$$\Lambda = \sqrt{\frac{I_1}{3}} = \sqrt{\frac{tr\left(\mathbf{F}^T\mathbf{F}\right)}{3}} \tag{4}$$

where I_1 is the first invariant of the right Cauchy green tensor $\mathbf{F}^T\mathbf{F}$.

If the material is incompressible and uniaxially stretched with three principal stretches ($\lambda_1 = \lambda, \lambda_2 = \lambda_3 = \lambda^{-1/2}$), the nominal stress along $\lambda_1$direction can be written as

$$s_1 = k_B T N_0 \sqrt{n_0} \frac{\left(\lambda - \lambda^{-2}\right)}{\sqrt{3\lambda^2 + 6\lambda^{-1}}} L^{-1}\left(\sqrt{\frac{\lambda^2 + 2\lambda^{-1}}{3n_0}} \right) \tag{5}$$

3.3. Uncrosslinked polymer chains

Unlike the covalent network, we assume the chain lengths of the uncrosslinked polymer chains are inhomogeneous. Considering the inhomogeneous chain length is to model the interpenetration behavior of the uncrosslinked charged chains

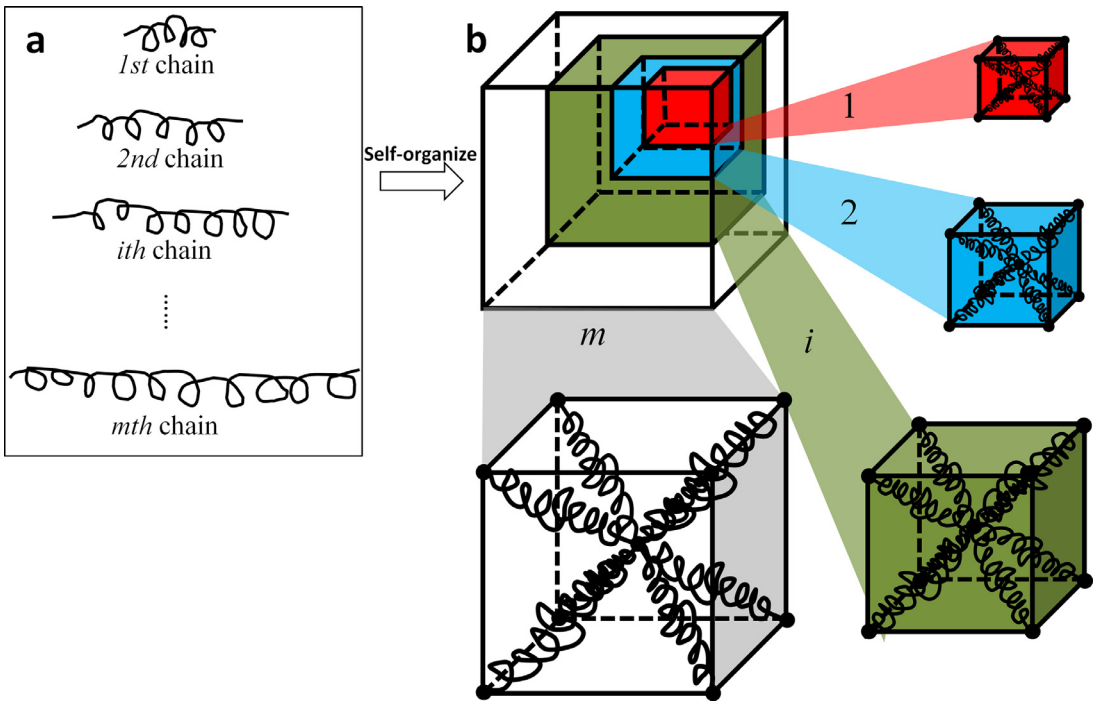

Fig. 4. (a) m types of polymer chains with different chain lengths. (b) Each type of polymer chains self-organizes into body-centered eight-chain structures, and all these eight-chain structures interpenetrate with each other.

because the chain diffusion is dependent on the chain length. For both cationic and anionic chains, they consist of m types of polymer chains, each with the same chain lengths (Fig. 4a). We denote the number of Kuhn segment on the ith chain is n_i (Kuhn length as b). Without loss of generality, the chain length follows a sequence law $n_1 \le n_2 ... n_i .. \le n_m$ for $1 \le i \le m$. The numbers of ith polymer chains per unit volume of the material are N_i^+ and N_i^- for cationic and anionic gels, respectively. The chain number follows statistical distributions as

$$P_i^+(n_i) = \frac{N_i^+}{\sum_{i=1}^m N_i^+}, \; P_i^-(n_i) = \frac{N_i^-}{\sum_{i=1}^m N_i^-} \tag{6}$$

For the undeformed ith chain, the end-to-end distance is $r_i^0 = \sqrt{n_i} b$. Under stretch, the deformed end-to-end distance is r_i with the corresponding chain stretch as

$$\Lambda_i = \frac{r_i}{r_i^0} \tag{7}$$

The free energy of the deformed ith chain is

$$w_i = n_i k_B T \left(\frac{\beta_i}{\tanh \beta_i} + \ln \frac{\beta_i}{\sinh \beta_i} \right) \tag{8}$$

where $\beta_i = L^{-1}(\Lambda_i / \sqrt{n_i})$. And the chain force on the deformed ith chain can thus be calculated as

$$f_i = \frac{\partial w_i}{\partial r_i} = \frac{k_B T}{b} \beta_i \tag{9}$$

3.4. Electrophoresis induced hydrogel adhesion

3.4.1. Electric field assisted reptation of a charged polymer chain

Let us first consider the penetration behavior of a charged polymer chain driven by an electric field (Fig. 5). We assume ith chain with n_i Kuhn segments and $n_i q$ charges. It moves along a reptation tube to diffuse (De Gennes, 1979; de Gennes, 1971; Doi and Edwards, 1978; Rubinstein and Colby, 2003). An electric field E is applied to promote the diffusion of the charged chain. We construct two coordinate systems: a curvilinear coordinate s along the chain reptation pathway and a linear coordinate y along the electric field direction (Fig. 5).

We first denote molar flux along the curvilinear coordinate s as Q_i (mol/m^2·s), and the molar concentration of the distal group on the ith chain as C_i (mol/m^3). Without loss of generality, C_i can be used to denote the chain with positive charges

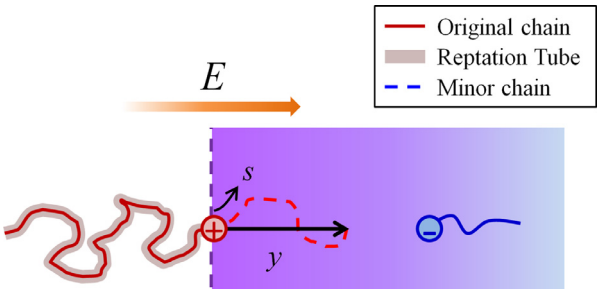

Fig. 5. Schematics to show the electrically-driven reptation of a charged polymer chain. The coordinate s is along the curvilinear contour of the newly-growing minor chain. The coordinate y is along the horizontal projection of the curvilinear coordinate s.

or negative charges. Conservation of mass yields

$$\frac{\partial C_i}{\partial t} = -\frac{\partial Q_i}{\partial s} \tag{10}$$

Then we employ the Stokes-Einstein model to consider the diffusion behavior from the molecular view (Grodzinsky, 2011). The basic idea is that the osmosis pressure gradient induced by the solute collision with the container wall is balanced by the friction force density during the molecular movement. Along the reptation tube, the friction force density is calculated as

$$g_i = (n_i \xi U - n_i qE\langle\cos\theta\rangle)(C_i N_{av}) \tag{11}$$

where ξ is the friction coefficient per Kuhn segment, U is the velocity of the Kuhn segment, $C_i N_{av}$ is molecule number per unit material volume, $n_i qE\cos\theta$ is the projection of electric force along the tube local coordinate, and θ is the angle between the electric field and the tangential direction of local coordinate s. $\langle\cos\theta\rangle$ is the statistical average along the whole chain. Following the model of DNA electrophoresis (Slater and Noolandi, 1986), we can calculate

$$\langle\cos\theta\rangle = \frac{qEb}{6k_BT} \tag{12}$$

To assist the understanding of this paper, we present the derivation process of Eq. (10) in the Appendix A following references (Lumpkin et al., 1985; Slater and Noolandi, 1986). Note that we here do not consider the chain as a semi-flexible chain like the DNA chain, but still consider a Gaussian random walk model under an electric field (Appendix A). Besides, we do not consider the free energy of the chain as that of the semi-flexible DNA chain.

The osmosis pressure is defined as (Grodzinsky, 2011)

$$P_o = RTC_i \tag{13}$$

where R is the universal gas constant, and the Boltzmann constant is $k_B = R/N_{av}$.

Considering the force balance between the friction force density and osmosis pressure gradient along the reptation tube, we obtain (Grodzinsky, 2011)

$$-\frac{\partial P_o}{\partial s} = -RT\frac{\partial C_i}{\partial s} = (n_i \xi U - n_i qE\langle\cos\theta\rangle)(C_i N_{av}) \tag{14}$$

Note that the molar flux at the molecular view can also be expressed as (Grodzinsky, 2011)

$$Q_i = C_i U \tag{15}$$

Therefore, from Eq. (14), we can express the molar flux as

$$Q_i = -\frac{k_BT}{n_i\xi}\frac{\partial C_i}{\partial s} + \frac{qE\langle\cos\theta\rangle}{\xi}C_i \tag{16}$$

Note that the Rouse dynamics diffusivity of the ith chain is (De Gennes, 1979; de Gennes, 1971; Doi and Edwards, 1978; Rubinstein and Colby, 2003).

$$D_i = \frac{k_BT}{n_i\xi} \tag{17}$$

Combining Eqs. (10), (12), (16) and (17), we obtain the equation for the electrically-driven diffusion of a charged polymer chain as

$$\frac{\partial C_i}{\partial t} = D_i\frac{\partial^2 C_i}{\partial s^2} - \frac{qE\langle\cos\theta\rangle}{\xi}\frac{\partial C_i}{\partial s} = D_i\frac{\partial^2 C_i}{\partial s^2} - \frac{bq^2E^2}{6k_BT\xi}\frac{\partial C_i}{\partial s} \tag{18}$$

If no electric field is applied, Eq. (18) is reduced to

$$\frac{\partial C_i}{\partial t} = D_i \frac{\partial^2 C_i}{\partial s^2} \tag{19}$$

which is the same as the curvilinear diffusion equation we obtained in the previous paper in modeling the self-healing mechanics of nanocomposite hydrogels (Wang et al., 2017). Here we derive the electric-assisted diffusion equation by adding the electric field term shown in Eq. (18).

Next question is how to convert the curvilinear coordinate s and the linear penetration coordinate y (Fig. 5). Following the model of DNA electrophoresis (Slater and Noolandi, 1986), we consider a 1D problem with

$$y = \sqrt{sb\left(1 - \frac{sbq^2E^2}{9k_B^2T^2}\right)^{-1}} \tag{20}$$

Eq. (20) can further be written as

$$\frac{s}{b} = \frac{\left(\frac{y}{b}\right)^2}{1 + \left(\frac{y}{b}\right)^2 \frac{b^2q^2E^2}{9k_B^2T^2}} \tag{21}$$

If the electric field is zero, Eq. (21) is reduced to $y \approx \sqrt{sb}$, which is the same as that in the previous paper without the application of the electric field (Wang et al., 2017).

3.4.2. Formation of the interpenetration region

The charged chains around the interface are driven by the electric field to penetrate into another material part (Fig. 1). Once the distal group of the cationic chain encounters the distal group of the anionic chain, an ionic bond will form. The formation of the ionic bond will subsequently affect the diffusion process of other chains. Therefore, the diffusion and the distal-group reaction are strongly coupled around the interface.

Let us first consider the distal group reaction. We denote the molar concentration of the end group in the ith cationic chain as C_i^+ (mol/m^3), and that of the ith anionic chain as C_i^- (mol/m^3). When a cationic distal group encounters an anionic distal group, they will form an ionic bond. Effectively, this reversible reaction can be denoted as Positive (P) + Negative (N) $\Leftrightarrow$ Ionic bond. The forward reaction will enable the association of the ionic bond, and the reverse reaction will enable the dissociation of the ionic bond. We further denote the molar concentrations of the dissociated distal groups as C_i^{+d} and C_i^{-d}, and the associated distal groups as C_i^{+a} and C_i^{-a}, respectively. The chemical reaction can be effectively written as

$$[+D] + [-D] \leftrightarrow [+A] + [-A] \tag{22}$$

where $[+D]$, $[-D]$, $[+A]$, and $[-A]$ are dissociated cationic, dissociated anionic, associated cationic, and associated anionic groups, respectively. We denote the forward reaction rate on the ith chain as k_i^f, and the reverse reaction rate on the ith chain as k_i^r. These reaction rates are chain-force dependent, as the chain force would promote the dissociation of the ionic bond (more details in Section 3.4.3). At the relaxed state, the reaction rates are reduced to those at the stress-free state k_i^{f0} and k_i^{r0}, respectively. The chemical kinetics can be written as (Hänggi et al., 1990; Kramers, 1940).

$$\frac{\partial C_i^{+a}}{\partial t} = \frac{\partial C_i^{-a}}{\partial t} = k_i^{f0} C_i^{+d} C_i^{-d} - k_i^{r0} C_i^{+a} C_i^{-a} \tag{23}$$

where C_i^{+a}, C_i^{-a}, C_i^{+d}, and C_i^{-d} are the molar concentration of associated cationic, associated anionic, dissociated cationic, and dissociated anionic groups, respectively. We focus our attention on charged hydrogels with good electrophoresis-induced adhesion capability, so that the ionic bonds can easily form under relatively mild conditions. This requirement implies that k_i^{r0} should be much smaller than k_i^{f0}, i.e., $k_i^{r0} << k_i^{f0}$. Under this condition, Eq. (23) is reduced as

$$\frac{\partial C_i^{+a}}{\partial t} = \frac{\partial C_i^{-a}}{\partial t} \approx k_i^{f0} C_i^{+d} C_i^{-d} \tag{24}$$

Note that physically speaking the reversible ionic bond should continuously undergo association and dissociation. However, we here consider $k_i^{r0} << k_i^{f0}$ such that the formed bond would effectively remain at the associated state until a mechanical or electrical force is applied. This character should be different from that of exchange reactions of dynamic covalent bonds (He et al., 2018; Yu et al., 2016).

Integrating the distal group reaction (Eq. (24)) and the chain diffusion (Eq. (18)), we can formulate the effective diffusion-reaction model as

$$\begin{cases} \frac{\partial C_i^{+d}}{\partial t} = D_i \frac{\partial^2 C_i^{+d}}{\partial s^2} - \frac{bq^{+2}E^2}{6k_BT\xi} \frac{\partial C_i^{+d}}{\partial s} - \frac{\partial C_i^{+a}}{\partial t} \\ \frac{\partial C_i^{+a}}{\partial t} \approx k_i^{f0} C_i^{+d} C_i^{-d} \end{cases} \tag{25}$$

$$\begin{cases} \frac{\partial C_i^{-d}}{\partial t} = D_i \frac{\partial^2 C_i^{-d}}{\partial s^2} - \frac{bq^{-2}E^2}{6k_BT\xi}\frac{\partial C_i^{-d}}{\partial s} - \frac{\partial C_i^{-a}}{\partial t} \\ \frac{\partial C_i^{-a}}{\partial t} \approx k_i^{f0} C_i^{+d} C_i^{-d} \end{cases} \tag{26}$$

where $n_i q^+$ and $n_i q^-$ are charge numbers of the ith cationic and anionic chains, respectively. Eqs. (25) and (26) can be reduced as

$$\begin{cases} \frac{\partial C_i^{+d}}{\partial t} = D_i \frac{\partial^2 C_i^{+d}}{\partial s^2} - \frac{bq^{+2}E^2}{6k_BT\xi}\frac{\partial C_i^{+d}}{\partial s} - k_i^{f0} C_i^{+d} C_i^{-d} \\ \frac{\partial C_i^{-d}}{\partial t} = D_i \frac{\partial^2 C_i^{-d}}{\partial s^2} - \frac{bq^{-2}E^2}{6k_BT\xi}\frac{\partial C_i^{-d}}{\partial s} - k_i^{f0} C_i^{+d} C_i^{-d} \end{cases} \tag{27}$$

We assume the diffusion and reaction only occur near the contact interface within a so-called "*interpenetration region*". We assume the width of this region is $2H$ with two boundaries as $y = \pm H$ (Fig. 1ab). In the curvilinear coordinate, the boundaries are $s = \pm s_H$, where s_H obtained from Eq. (21). We assume the boundary conditions at any time t can be expressed as

$$C_i^{+d}(s = -s_H, t) = N_i^+,\ C_i^{+d}(s = s_H, t) = 0 \tag{28a}$$

$$C_i^{-d}(s = s_H, t) = N_i^-,\ C_i^{-d}(s = -s_H, t) = 0 \tag{28b}$$

where N_i^+ and N_i^- are the concentration of the initial dissociated ith cationic and anionic chains, respectively. Note that H should be small enough to show the interpenetration region is only located around the interface, and at the same time, it should be large enough to fulfill the boundary condition Eq. (28). At the beginning of the interpenetration process, the ith cationic chain only exists in the left part of the material, and the ith anionic chain only exists in the right part (Fig. 1b). This can be expressed as

$$C_i^{+d}(s, t = 0) = N_i^+ \Psi(s) \tag{29a}$$

$$C_i^{-d}(s, t = 0) = N_i^- [1 - \Psi(s)] \tag{29b}$$

where $\Psi(s)$ is a step function with a definition as $\Psi(s) = 1$ at $s > 0$, $\Psi(s) = 0.5$ at $s = 0$, and $\Psi(s) = 0$ at $s < 0$.

With Eqs. (27)-(28), we can formulate the molar concentration of dissociated $C_i^{+d}(s, t)$ and $C_i^{+d}(s, t)$. The molar concentration of the associated ith chain is

$$C_i^{+a}(s, t) = C_i^{-a}(s, t) \approx \int_0^t k_i^{f0} C_i^{+d}(s, \tau) C_i^{-d}(s, \tau) d\tau \tag{30}$$

The effective volume density of the active ith cationic chains $N_i^{+ha}(t)$ and anionic chains $N_i^{-ha}(t)$ within the interpenetration region can be estimated as an average within the region $s = [-s_H, s_H]$, written as,

$$N_i^{+ha}(t) = N_i^{-ha}(t) = \frac{1}{2s_H} \int_{-s_H}^{s_H} C_i^{+a}(s, t) ds \tag{31}$$

Since ith cationic and anionic chains have the same chain length, the effective volume density of the active ith chain N_i^{ha} within the interpenetration region can thus be estimated as

$$N_i^{ha}(t) = N_i^{+ha}(t) + N_i^{-ha}(t) \tag{32}$$

3.4.3. Deformation of the interpenetration region

After the electrophoresis process, the sample becomes a composite with part A region, interpenetration region and part B region. The mechanical behaviors of part A and part B are modeled in Section 3.2. The mechanical property of the interpenetration region is modeled as follows.

Similar to the Arruda–Boyce model, we assume the linked active ith chains self-organize into body-centered eight-chain structures (Fig. 4b) (Arruda and Boyce, 1993; Rubinstein and Colby, 2003; Treloar, 1975). The material follows an affined deformation model (Arruda and Boyce, 1993; Rubinstein and Colby, 2003; Treloar, 1975), so that under the deformation gradient $\mathbf{F}$ the stretch of the ith chain is

$$\Lambda_i = \sqrt{\frac{I_1}{3}} = \sqrt{\frac{tr\left(\mathbf{F}^T\mathbf{F}\right)}{3}} \tag{33}$$

When the part A and part B are under a tensile load, the interpenetration region is under a shear deformation (Fig. 3a). The deformation gradient can be expressed as

$$\mathbf{F} = \begin{bmatrix} 1 & & 0 \\ \lambda^H & 1 & 0 \\ 0 & 0 & 1 \end{bmatrix} \tag{34}$$

where λ^H is the shear stretch. The right Cauchy green tensor is

$$\mathbf{C} = \mathbf{F}^T\mathbf{F} = \begin{bmatrix} 1 & \lambda^H & 0 \\ \lambda^H & \lambda^{H2}+1 & 0 \\ 0 & 0 & 1 \end{bmatrix} \tag{35}$$

The first invariant of the right Cauchy green tensor is

$$I_1 = tr(\mathbf{C}) = \lambda^{H2} + 3 \tag{36}$$

At the stress-free state, the volume density of the active ith chain $C_i^{+a}(s,t) = C_i^{-a}(s,t) \approx \int_0^t k_i^{f0} C_i^{+d}(s,\tau) C_i^{-d}(s,\tau) d\tau$ within the interpenetrated region can be calculated from Eq. (30). Under deformation, the volume density of the active ith chain within the interpenetrated region reduces to N_i^{ha}. Similar to Eq. (3), the free energy density of the deformed interpenetrated region can be formulated as

$$W^H = W_{mix}^H + \sum_{i=1}^{m} N_i^{haa} n_i k_B T \left(\frac{\beta_i}{\tanh\beta_i} + \ln\frac{\beta_i}{\sinh\beta_i} \right) \tag{37}$$

$$\beta_i = L^{-1}\left(\sqrt{\frac{I_1}{3n_i}}\right) = L^{-1}\left(\sqrt{\frac{\lambda^{H2}+3}{3n_i}}\right) \tag{38}$$

where W_{mix}^H is assumed as constant. The shear stress can be formulated as

$$s_{12}^H = \frac{\partial W^H}{\partial \lambda^H} = \sum_{i=1}^{m} \frac{2N_i^{haa}\sqrt{n_i} k_B T \beta_i \lambda^H}{3} \tag{39}$$

where β_i is given in Eq. (38).

Another issue is that the active ith chain number will decrease as the deformation is applied. To calculate the active ith chain volume density N_i^{haa} (shown in Eq. (37)), we employ a Bell-like force-dependent reaction model (Bell, 1978; Ribas-Arino and Marx, 2012). The force would promote the dissociation of the ionic bond. We denote the volume density of the associated and dissociated ith positive chains as N_i^{+haa} and N_i^{+had}, ith negative chains as N_i^{-haa} and N_i^{-had}, respectively. Similar to Eq. (23), we can formulate the chemical kinetics at the deformed state as

$$\frac{\partial N_i^{+haa}}{\partial t} = \frac{\partial N_i^{-haa}}{\partial t} = k_i^f N_i^{+had} N_i^{-had} - k_i^r N_i^{+haa} N_i^{-haa} \tag{40}$$

The forward reaction rate (from the dissociated state to the associated state) is k_i^f and reverse reaction rate is k_i^r when the chain is stretched. Following the Bell model, we consider an energy barrier exists between the associated state and dissociated state through a transition state (Bell, 1978; Ribas-Arino and Marx, 2012). There are energy barriers between associated (A) and dissociated (D) states. The chain force effectively alters the potential energy landscape of the dissociation-association reaction: The chain force lowers down the energy barrier of A $\rightarrow$ D and increases the energy barrier for D $\rightarrow$ A. The reaction rates are governed by the energy barrier through exponential functions as (Bell, 1978; Ribas-Arino and Marx, 2012)

$$k_i^f = k_i^{f0} \exp\left(-\frac{f_i \Delta x}{k_B T}\right) \tag{41a}$$

$$k_i^r = k_i^{r0} \exp\left(\frac{f_i \Delta x}{k_B T}\right) \tag{41b}$$

where f_i is the chain force of the associated chain, k_i^{f0} and k_i^{r0} are reaction rates at the stress-free state, and Δx is the distance along the energy landscape coordinate. Δx will be treated as a fitting parameter in the model. Note that this Bell model considers an effective behavior and the chain force f_i in Eq. (41a) is onsidered as that of the associated chain.

According to Eq. (7), the chain force is

$$f_i = \frac{k_B T}{b}\beta_i = \frac{k_B T}{b} L^{-1}\left(\sqrt{\frac{\lambda^{H2}+3}{3n_i}}\right) \tag{42}$$

In a quasi-static loading, we assume that the loading is so slow that the chemical reaction reaches the equilibrium state at any small increment of strains. Under this loading, we consider the time-dependent terms in Eq. (40) disappear, and Eq. (40) can be reduced as

$$k_i^f N_i^{+had} N_i^{-had} - k_i^r N_i^{+haa} N_i^{-haa} = 0 \tag{43}$$

Note that the reduction from Eqs. (40) to (43) is based on the estimation of the time scale of Eq. (40). The time scale of Eq. (40) can be roughly estimated as $1/(k_i^r N_i^{ha})$, where $k_i^r \sim 2\times10^{-6}$–$1\times10^{-4}$ $m^3{\cdot}s^{-1}$ and $N_i^{ha} \sim 10^{-10}$–10^{-4} $mol{\cdot}m^{-3}$. The

resultant time scale of Eq. (40) (e.g., 10^{-9} s) is much smaller than the time scale of each strain increase step during the experiment ($\sim 10^{-3}$ s). Also, the reduction from Eqs. (40) to (43) may only be applied to the behavior before the breaking of the bonded interface. However, we may only be interested in the behavior before the interface breaking. Considering the conservation $N_i^{+had} + N_i^{+haa} = N_i^{+ha}$ and $N_i^{-had} + N_i^{-haa} = N_i^{-ha}$, the active ith chain volume density can be calculated as

$$N_i^{haa} = \frac{N_i^{ha}\sqrt{k_i^r}}{\sqrt{k_i^f} + \sqrt{k_i^r}} = \frac{N_i^{ha}\sqrt{k_i^{r0}\exp\left(-\frac{f_i\Delta x}{k_BT}\right)}}{\sqrt{k_i^{f0}\exp\left(\frac{f_i\Delta x}{k_BT}\right)} + \sqrt{k_i^{r0}\exp\left(-\frac{f_i\Delta x}{k_BT}\right)}} \tag{44}$$

3.5. Electrophoresis induced adhesion releasing

An electric field E_1 is first applied to treat the sample for time t_1 to enable the hydrogel adhesion and then use an electric field E_2 with the reverse direction to release the adhesion (Fig. 1c). When an electric field with the reverse direction is applied, the electric force will drag the associated ionic bones open and charged chain will gradually move in the reverse direction driven by the electric field (Fig. 1d). Therefore, the reverse electrophoresis process around the interface is also a coupled diffusion-reaction behavior.

Following Section 3.4.2, we can write the governing equation of the reverse electrophoresis process as

$$\begin{cases} \dfrac{\partial C_i^{+d}}{\partial t} = D_i\dfrac{\partial^2 C_i^{+d}}{\partial s^2} + \dfrac{bq^{+2}E^2}{6k_BT\xi}\dfrac{\partial C_i^{+d}}{\partial s} - \dfrac{\partial C_i^{+a}}{\partial t} \\ \dfrac{\partial C_i^{+a}}{\partial t} = k_i^f C_i^{+d} C_i^{-d} - k_i^r C_i^{+a} C_i^{-a} \end{cases} \tag{45a}$$

$$\begin{cases} \dfrac{\partial C_i^{-d}}{\partial t} = D_i\dfrac{\partial^2 C_i^{-d}}{\partial s^2} + \dfrac{bq^{-2}E^2}{6k_BT\xi}\dfrac{\partial C_i^{-d}}{\partial s} - \dfrac{\partial C_i^{-a}}{\partial t} \\ \dfrac{\partial C_i^{-a}}{\partial t} k_i^f C_i^{+d} C_i^{-d} - k_i^r C_i^{+a} C_i^{-a} \end{cases} \tag{45b}$$

The sign in front of the term $bq^{+2}E^2/(6k_BT\xi)$ is different from those in Eqs. (25) and (26), because the electric field direction is reversed. The reaction rates are affected by the electric force through Eq. (41) written as $k_i^f = k_i^{f0}\exp(-f_i\Delta x/k_BT)$ and $k_i^r = k_i^{r0}\exp(f_i\Delta x/k_BT)$, where the electrically-induced average chain force is

$$f_i = n_i q E_2 \langle\cos\theta\rangle = \frac{n_i q^2 E_2^2 b}{6k_BT} \tag{46}$$

where the average charge value is estimated as $q = (q^+ + q^-)/2$. Δx is the same parameter used in Section 3.4.3. The boundary conditions for Eq. (45) within the region $y = [-H, H]$ (or $s = [-s_H, s_H]$) are the same as Eq. (28). And the initial condition of Eq. (45) is the concentration distribution after the electrophoresis process with electric field E_1 for time t_1.

4. Theoretical results

4.1. Polymer chain interpenetration

The polymer chain interpenetration behavior is modeled in Section 3.4.2. Solving Eqs. (27)-(28), we can obtain the distribution of the concentration of the dissociated distal group of the cationic ith chain $C_i^{+d}(s,t)$ over the curvilinear coordinate s for various normalized electrophoresis time $\tilde{t} = tk_BT/(n_i\xi s_H^2)$ (Fig. 6a). Note that all used parameters for the calculations are given in Table 1. Initially, the dissociated distal group of the cationic ith chains only exist at $s < 0$. With increasing electrophoresis time, the cationic ith chains interpenetrate into $s > 0$. Accordingly, the associated cationic ith chain form when the dissociated cationic ith chain encounters dissociated anionic ith chain. The concentration of the associated ith chain from Eq. (30) and the corresponding volume density of the active ith chain within the interpenetrated region can thus be calculated from Eq. (31) and shown in Fig. 6b (The calculation is based on $N_i^+ = N_i^- = N_i$ and $q^+ = q^-$). The active ith chain density increases with increasing electrophoresis time and gradually reaches a plateau when the electrophoresis time is long enough.

4.2. Electrophoresis-induced hydrogel adhesion

We employ the interpenetration network model described in Section 3.3 to model the electrophoresis-induced hydrogel adhesion. For the sake of simplicity of analysis, we assume the m types of ith chain follow a log-normal chain-length

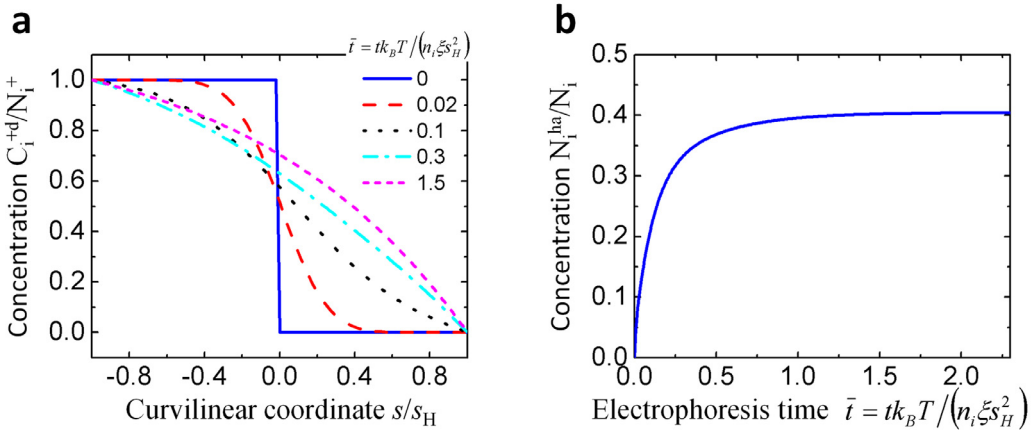

Fig. 6. (a) The distribution of the concentration of the dissociated distal group of the cationic ith chain over the curvilinear coordinate for various normalized electrophoresis time $\bar{t} = tk_BT/(n_i\xi s_H^2)$. (b) The volume density of the active cationic ith chain within the interpenetrated region as a function of the normalized electrophoresis time $\bar{t} = tk_BT/(n_i\xi s_H^2)$. The calculation is based on $N_i^+ = N_i^- = N_i$ and $q^+ = q^-$. The used parameters can be found in Table 1.

distribution as

$$P_i^+(n_i) = P_i^-(n_i) = \frac{1}{n_i\delta\sqrt{2\pi}} \exp\left[-\frac{(\ln n_i - \ln n_a)^2}{2\delta^2}\right] \tag{47}$$

where n_a and δ are the mean of n_i and standard deviation of $\ln n_i$, respectively. A typical chain length distribution is shown in Fig. 7a. According to Eq. (6), we assume

$$N_i^- = \alpha N_i^+ \tag{48}$$

where α is a coefficient to indicate the relative density ratio between the anionic chains and cationic chains. Considering that the mechanical properties of the two hydrogels are almost the same (Fig. 12a) and applied molar amounts of Chitosan and PGA are close, we make a bold assumption with $\alpha = 1$. Also, according to the molecular structures shown in Fig. 2, we further assume $q^+ = q^- = q$. These assumptions are just for the sake of the analysis simplicity; the analysis with other value of N_i^{-hara} and dissimilar charge values can be easily carried out based on the model shown in Section 3.

With a calculated associated chain density N_i^{ah} at a given electrophoresis time t (Fig. 6b), we can go through Section 3.4.3 to calculate the shear force F with increasing shear stretch λ^H of the interpenetration segment (Fig. 7b). It is noted that employing an inhomogeneous chain-length distribution has a special advantage in the determination of the shear strength. The shear force first increases with the shear stretch and then decrease with a maximal point; because as the shear stretch increases, the associated chains will be gradually dissociated. The shorter chains are dissociated first as their chain forces are larger, and then longer chains. Once the active chain number decreases to a certain extent, the interpenetration segment cannot sustain the applied shear force so the shear force begins to decrease. Experimentally, at this maximal point, the interpenetration segment is ruptured, and the corresponding shear stress is the shear strength.

Considering the force balance $F/L_w = s_{12}^H L_d = s_1 L_t$ shown in Eq. (2) (Fig. 7cd), we can obtain the relationship between the uniaxial force F/L_w and uniaxial strain ε of the electrophoresis-treated sample (Fig. 7e). Collecting the maximal uniaxial forces and converting to the shear stress $s_{12}^H = F/(L_w L_d)$, we can obtain a relationship between the shear strength s_{12}^{Hm} and the electrophoresis time t (Fig. 7f). The predicted shear strength increases as the electrophoresis time t increases and reaches a plateau when t is long enough. We define the equilibrium electrophoresis time t_{eq} as the electrophoresis time corresponding to 90% of the plateau value.

4.2.1. Effect of electric force Eq

We first study the effect of the electric force Eq on the electrophoresis-induced hydrogel adhesion. According to Section 3, we can calculate the shear strength of the interpenetration region as a function of the electrophoresis time for various normalized electric forces Eqb/k_BT (Fig. 8a). The corresponding equilibrium shear strength at the plateau and equilibrium electrophoresis time are plotted as functions of Eqb/k_BT (Fig. 8bc). It is found that the equilibrium shear strength increases with increasing electric force because the higher electric force would drive more chains to interpenetrate into each other to form more active chains across the interface. It is also found that the equilibrium electrophoresis time first increases with the electric force and then decrease until a plateau at an infinitely small value. This counterintuitive phenomenon can be understood as follows: When the electric force is small, chains move slowly across the interface; while a larger amount of active chains are required to reach the plateau as the electric force increases; therefore, a longer electrophoresis time is required to drive enough chains across the interface as the electric force is larger. However, when the electric fore is large enough, the chains move quickly, and sufficient chains can move across the interface within a short time.

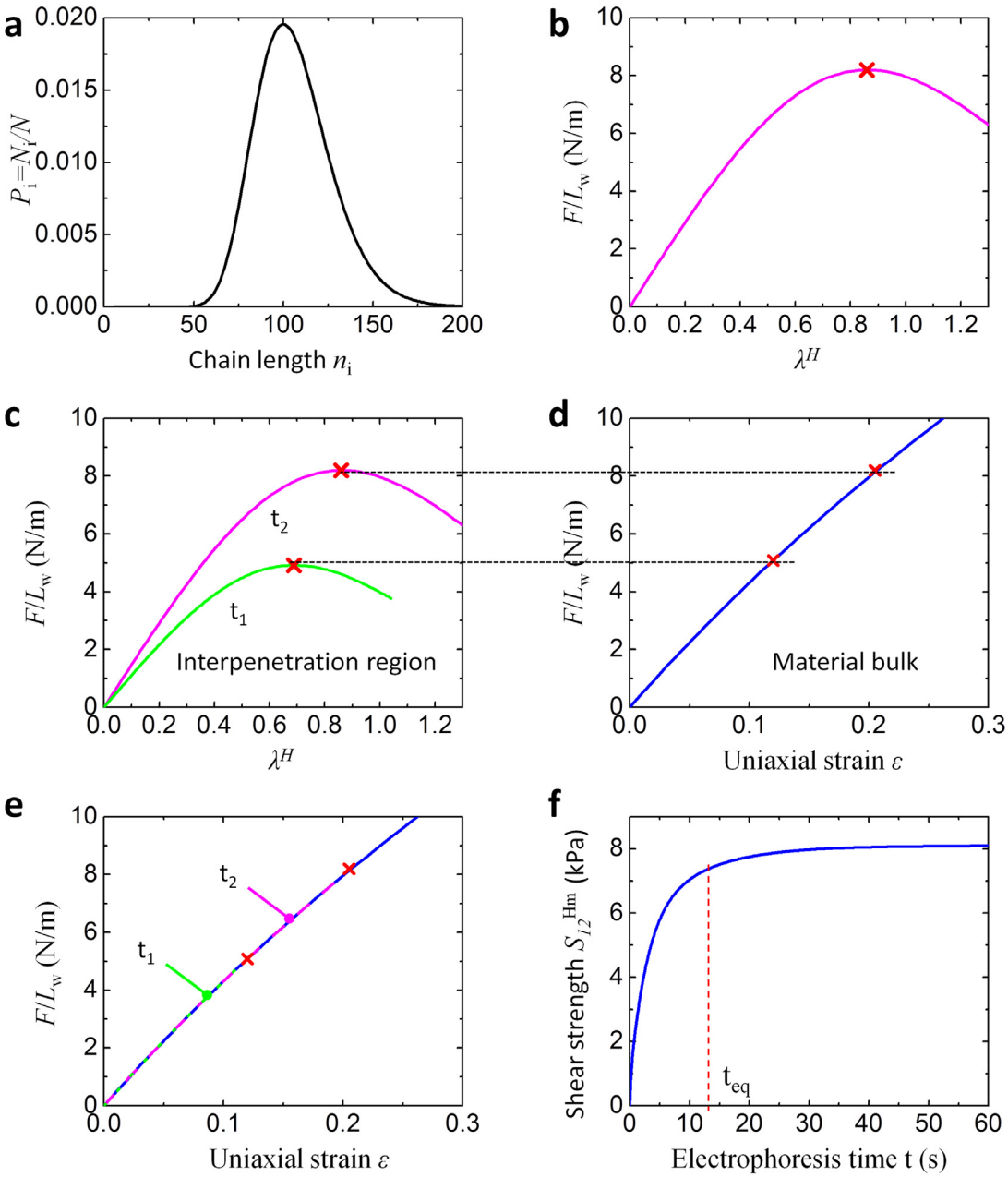

Fig. 7. (a) The chain length distribution for the interpenetration region. (b) A typical shear force-shear stretch of the interpenetration region. As the shear stretch increases, the shear force first increases and then decreases because of the dissociation of the associated chains. (cd) The shear force of the interpenetration region (c) should be equal to the uniaxial force in the material bulk region (d). Based on the interaction of (c) and (d), the resultant uniaxial force-uniaxial strain relationship can be obtained for the sample after the electrophoresis of various time (e). Collecting the critical points denoted by the red cross for various electrophoresis time in (f), the relationship between the shear strength of the sample and the electrophoresis time can be predicted. The equilibrium electrophoresis time t_{eq} is corresponding to 90% of the plateau value. The used parameters can be found in Table 1.

4.2.2. Effect of Rouse friction coefficient

Then, we study the effect of Rouse friction coefficient ξ on the electrophoresis-induced hydrogel adhesion. As shown in Eq. (27), coefficients in the diffusion term ($D_i = k_BT/(n_i\xi)$) and the convection term ($bq^2E^2/(6k_BT\xi)$) are dependent on the friction coefficient ξ. After plotting the shear strengths in functions of electrophoresis time for various friction coefficients ξ (Fig. 9a), we find that the friction coefficient does not affect the equilibrium shear strength and that the equilibrium electrophoresis time increases as the friction coefficient increases (Fig. 9b). It is because that higher friction of the chain movement will lead to a longer time to reach the equilibrium state.

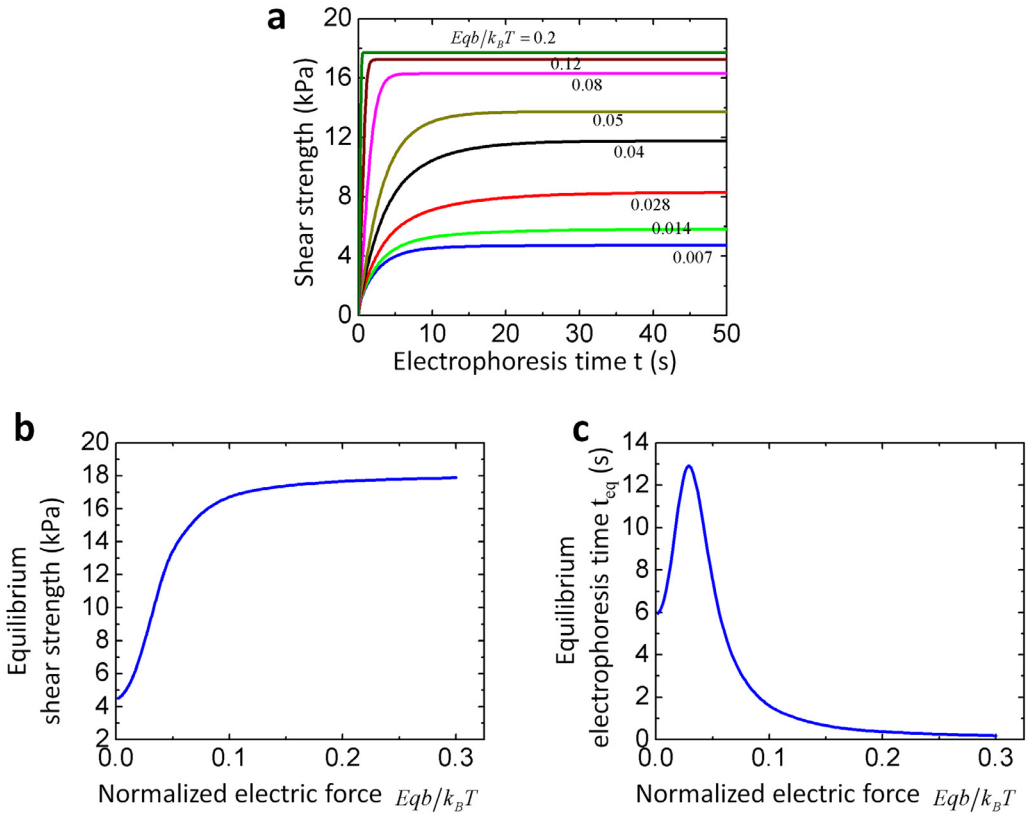

Fig. 8. Effect of the electric force on the electrophoresis-induced hydrogel adhesion. (a) The shear strength as a function of the electrophoresis time for various normalized electric forces Eqb/k_BT. (b) The equilibrium shear strength as a function of the normalized electric force. (c) The equilibrium electrophoresis time as a function of the normalized electric force. The used parameters can be found in Table 1.

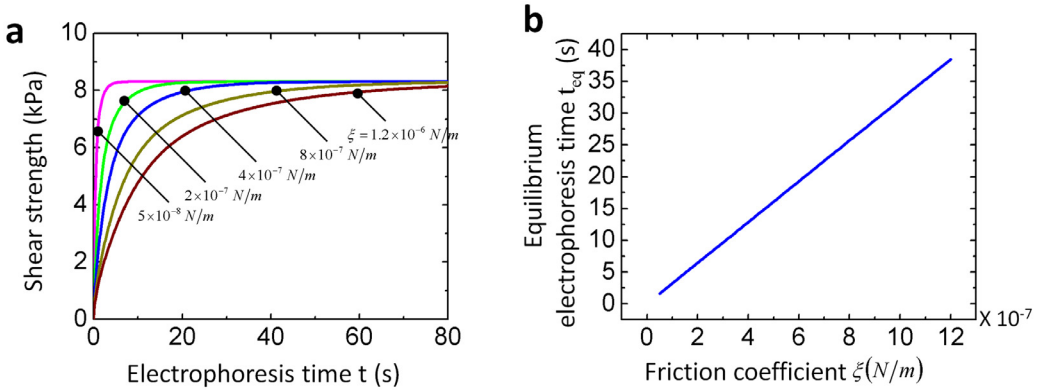

Fig. 9. Effect of the Rouse friction coefficient on the electrophoresis-induced hydrogel adhesion. (a) The shear strength as a function of the electrophoresis time for various Rouse friction coefficients. (b) The equilibrium electrophoresis time as a function of the Rouse friction coefficient. The used parameters can be found in Table 1.

4.2.3. Effect of chain length

Next, we study the effect of chain length on the electrophoresis-induced hydrogel adhesion. The chain length within the interpenetration region follows a log-normal distribution. To study the effect of chain length, we here only vary the average chain length of the chain-length distribution (Fig 10a). For various chain-length distributions, we can calculate the shear strengths of the interpenetration region as functions of the electrophoresis time (Fig. 10b). We find that both equilibrium shear strength and equilibrium electrophoresis time increase with increasing average chain lengths n_a (Fig. 10cd). It is because that as the average chain length increases, the effective Rouse diffusivity $D_i = k_BT/(n_i\xi)$ decreases, while the coefficient of the electric-force induced convection $bq^2E^2/(6k_BT\xi)$ remains. Lower chain diffusivity leads to a longer time to

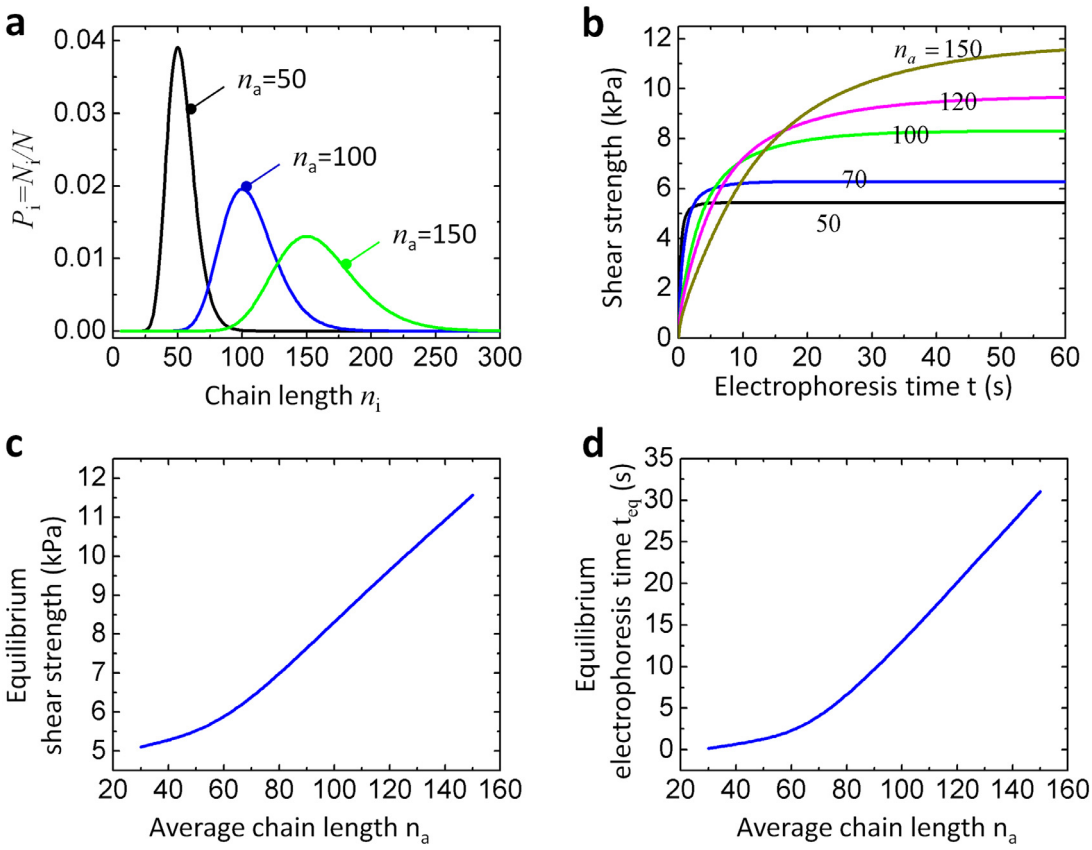

Fig. 10. Effect of the chain length on the electrophoresis-induced hydrogel adhesion. (a) Chain length distributions for various average chain lengths. (b) The shear strength as a function of the electrophoresis time for various average chain lengths. (c) The equilibrium shear strength as a function of the average chain length. (d) The equilibrium electrophoresis time as a function of the average chain length. The used parameters can be found in Table 1.

reach the equilibrium plateau. And within a longer time, more chains are driven by the electric field to cross the interface to form active chains. Therefore, both equilibrium shear strength and equilibrium electrophoresis time increase as the average chain length increases.

4.3. Electrophoresis-enabled adhesion releasing

After the electrophoresis process with increased hydrogel adhesion, the adhesion can be released if the electrophoresis voltage direction is reversed. Given a reverse electric field E_2, we calculate the volume density of the active *i*th chain within the interpenetration region for various reverse electrophoresis time (Fig. 11a). As shown in Fig. 11a that is calculated based on Fig. 6b, the volume density of the active *i*th chain decreases from an initial value as the reverse electrophoresis time increases. We then go through the calculation in Section 3.4.3 to calculate shear force within the interpenetration region (Fig. 11b), and then interact with the uniaxial force within the material bulk (Fig. 11c); and we thus obtain the sample shear strengths for various reverse electrophoresis time (Fig. 11d). As seen from Fig. 11d, the shear strength decreases with increase reverse electrophoresis time and then reaches a plateau when the reverse electrophoresis time is long enough.

5. Comparison with experimental results

To verify the theory, we compare the theoretical results with the experimental measurements. As a proof of concept, we employ gelatin-Chitason hydrogel as the cationic hydrogel and gelatin-PGA hydrogel as the anionic hydrogel. The uniaxial stress-strain behaviors of these two hydrogels are very similar below the strain 0.35 and nominal stress 12 kPa (Fig. 12a). Fortunately, the measured shear strengths of the tested samples are almost below 12 kPa. Therefore, we approximately assume that the mechanical properties of parts A and B are the same below 12 kPa, and can be captured using the same theory shown in Section 3.2.

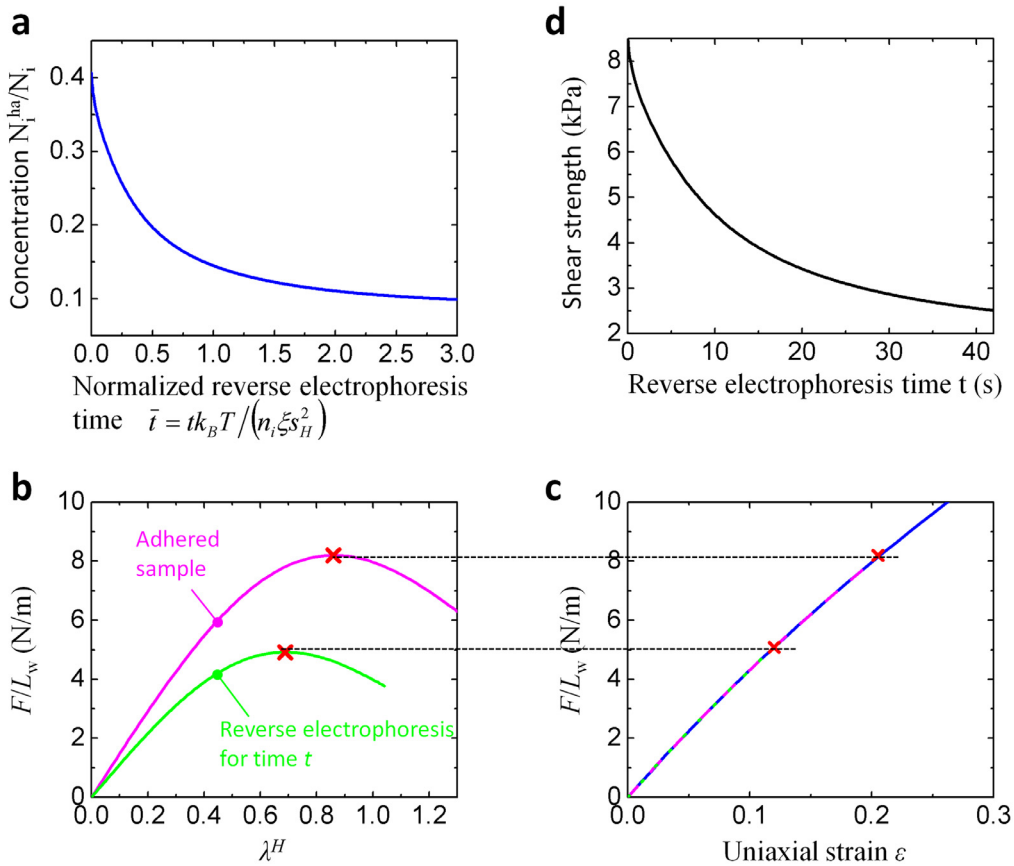

Fig. 11. Reverse electrophoresis induced adhesion releasing. (a) The volume density of the active cationic *i*th chain as a function of the normalized reverse electrophoresis time $\bar{t} = tk_BT/(n_i\xi s_H^2)$. (bc) The shear force of the interpenetration region (b) should be equal to the uniaxial force in the material bulk region (c). Based on the interaction of (b) and (c), the resultant uniaxial force-uniaxial strain relationship can be obtained for the sample after the electrophoresis of various time. (d) The predicted shear strength as a function of reverse electrophoresis time. The used parameters can be found in Table 1.

5.1. Electrophoresis enabled adhesion

Then, we use the gelatin-Chitason and gelatin-PGA hydrogels to carry out the electrophoresis experiment. We find that the uniaxial stress-strain curves collapse with only the maximal strength changes for various electrophoresis time. The uniaxial force-strain curves can be roughly matched with the theoretical results shown in Fig. 12b. The spikes in the experimental force-strain curves may come from the defects on the bonding interface. The corresponding shear strength for various electrophoresis time can also roughly matched with the theoretical calculations (Fig. 12c). The discrepancy in the short electrophoresis time may be because that we do not consider the instantaneous adhesion between two hydrogel samples. According to the theory, the shear strength should be equal to zero when the electrophoresis time is zero; however, the employ two employed hydrogel samples indeed show an instantaneous adhesion around 2-3 kPa.

Besides, we vary the applied electric field from 1 V/mm to 4 V/mm. We did not further increase the voltage because higher voltage may induce relatively strong chemical reactions of the hydrogels, which we do not consider in the theoretical model. We find that the shear strength-electrophoresis time for various electric fields (1-4 V/mm) can be roughly matched with the theoretical calculations (Fig. 13a). Again, the initial part of the strength-time curve may not be explained by the theory due to the instantaneous adhesion. However, the experimentally measured equilibrium shear strength can be explained by the theoretically calculated results (Fig. 13b). Besides, the experiments can verify the theoretical trend discussed in Section 4.2.1: the equilibrium electrophoresis time first increases with the applied electric field and then decreases (Fig. 13c). The measured results can roughly match the theoretical trend. The discrepancy in the low electric field range (<2 V/mm) may be due to the inevitable experimental error within 1-3 s as the equilibrium electrophoresis time is 4-7 s.

5.2. Reverse electrophoresis enabled adhesion releasing

After the electrophoresis process with 4 V/mm for around 40 s, the shear strength of the hydrogel bonding reaches around 8.3 kPa (Fig. 12c). Then, we apply a negative electric field (−1, −2, or −4 V/mm) to trigger the reverse electrophoresis process

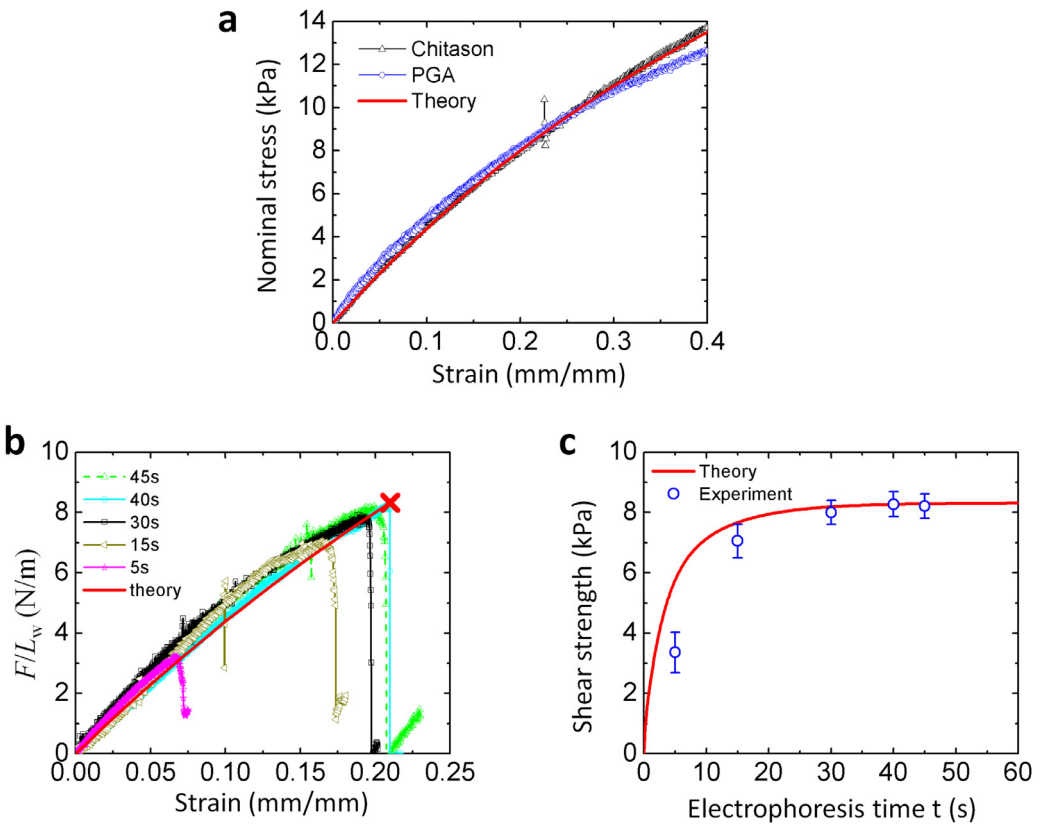

Fig. 12. (a) The nominal uniaxial stress of Chitosan and PGA hydrogels as functions of uniaxial strain. (b) The loading forces of samples with various electrophoresis time as functions of the uniaxial strain. The red crosses denote the predicted maximal loading forces corresponding to respective electrophoresis time. (c) The experimentally measured and theoretically calculated shear strength as functions of the electrophoresis time. For (a), the used parameters include $n_0 = 100$ and $N_0 k_B T = 48$. Other used parameters can be found in Table 1.

to release the formed adhesion. We find that the shear strength decreases as the reverse electrophoresis time increases, and that the adhesion release is more rapid for higher reverse electrophoresis voltage (Fig. 14). Quantitatively, the theoretical results can roughly match the experimentally measured shear strength as functions of the reverse electrophoresis time for various reverse voltages. In the small reverse electrophoresis time-scale, the theoretically calculated results are lower than the experimentally measured one. It shows that the decreasing of the experimentally measured interfacial bonding is slower than the theoretically modeled. This discrepancy may come from the contribution of the chain entanglement effect in the experiment: The electric field may first need to overcome the chain entanglement to trigger the chain to move apart, while the chain entanglement effect is not considered in the current model (De Gennes, 1979; de Gennes, 1971; Doi and Edwards, 1978; Rubinstein and Colby, 2003).

6. Conclusive remarks

In summary, we present an analytical theory framework to model the electrophoresis enabled reversible adhesion. We consider that during the electrophoresis process, free charged chains are driven by the electric field to move across the interface to interpenetrate into each other material matrix, and form weak ionic bonds with chains with opposite charges. We model the interpenetration process as a diffusion-reaction process with the chain diffusion modeled as an electrically-driven reptation-like motion and the cationic-anionic bond formation as a bell-like chemical reaction. We can theoretically depict the electrophoresis-induced hydrogel adhesion that is in a function of the electrophoresis time in an error-function fashion. We also predict that the hydrogel adhesion can be released by an electrophoresis process with reverse voltages. The theoretically calculated results can agree well with the experiments for both electrophoresis-induced hydrogel adhesion and adhesion releasing. The present model can be extended to explain the electric-field-assisted self-healing of charged soft polymers. The model may also provide insights into electroadhesion of soft elastomers that has been widely used in the designs of robotics or micromechanical systems.

We also notice that the present model has a large room for future improvement. First, a number of assumptions can be easily relaxed for more general systems. For example, we assume $N_i^+ = N_i^-$ and $q^+ = q^-$ through all the calculations, but these two conditions can be easily removed to account for the more general situations. As another example, we employ

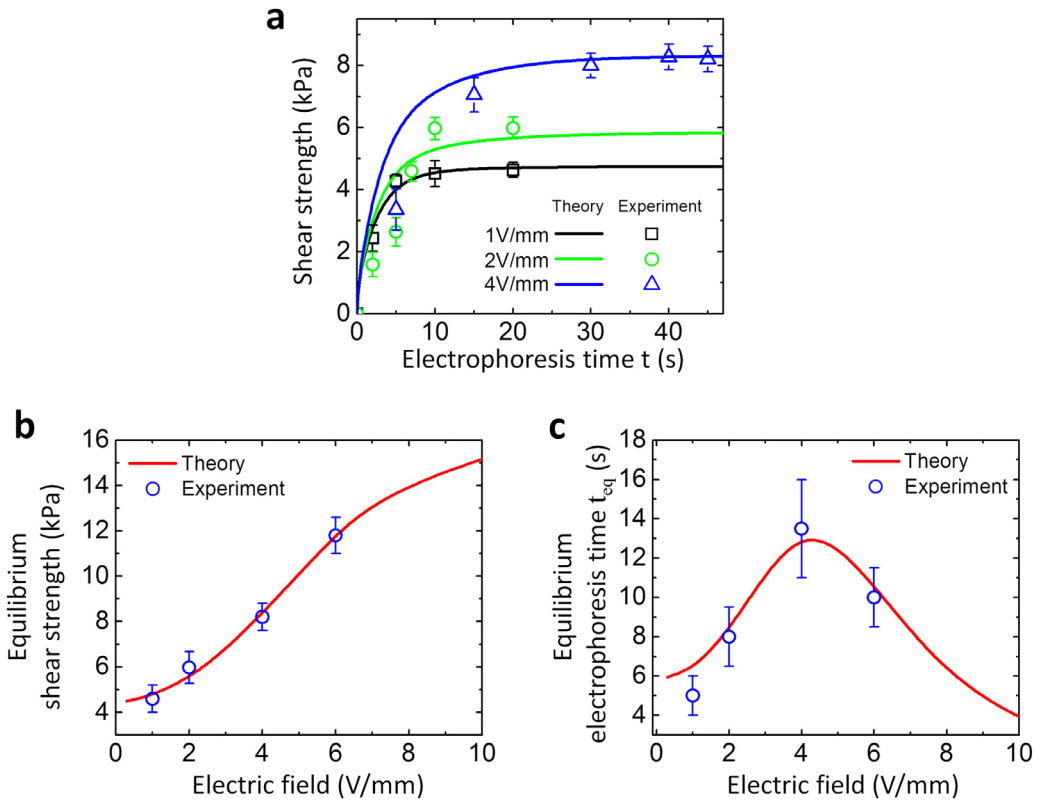

Fig. 13. The comparison between the theory and experiments on the effect of applied voltage on the electrophoresis-induced hydrogel adhesion. (a) The electrophoresis-induced shear strengths of samples with various applied electric fields as functions of the electrophoresis time. (b) The experimentally measured and theoretically calculated equilibrium shear strength as functions of the applied electric fields. (c) The experimentally measured and theoretically calculated equilibrium electrophoresis time as functions of the applied electric field. The used parameters can be found in Table 1.

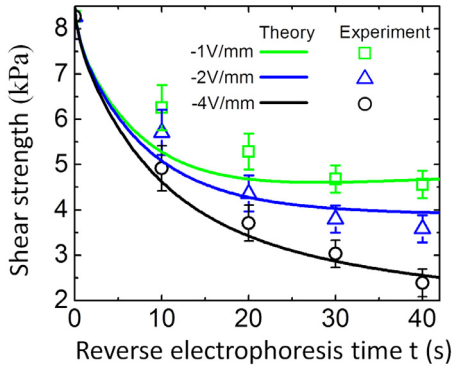

Fig. 14. The experimentally measured and theoretically calculated equilibrium shear strength as functions of the reverse electrophoresis time for various reverse voltages. The used parameters can be found in Table 1.

the log-normal chain-length distribution, but other chain length distributions such as normal distribution, log-logistic distribution, and Weibull distribution should also work for our model system (Wang et al., 2015). Second, we assume that the cationic *i*th chains only form ionic bonds with anionic chains with the same chain length. The assumption is only for the sake of computational simplicity. If the *i*th chain can be linked with the *j*th chain ($i \neq j$), the same chain force may induce imbalanced chain stretch in the *i*th chain and *j*th chain; therefore, a more generic statistical average algorithm is required to account for the effective behavior. Third, as discussed in Section 5.1, we do not consider the instantaneous adhesion of two hydrogel samples, which contributes to the results discrepancy between the theory and experiments when the electrophoresis time is short. We expect that future model can incorporate this effect into consideration.

Finally, our model only considers that a charged chain can only form one bond with the other charged chain. The process is shown in Fig. 15ab. Within this framework, the increase of the interfacial strength over time is induced by bonding more

Table 1
Definition and value of the employed parameters. The forward and reverse reaction rates are estimated based on the study regarding the polymer chains crosslinked by ionic bonds in (Wang et al., 2017; Yu et al., 2018). Δx is a fitting parameter to match the shear strength of the shear-lag samples. n_a is another fitting parameter to match the stress-strain behaviors of the samples. n_1 and n_m are two parameters chosen based on the value of n_a. ξ is the third fitting parameter to match the time scale of the electrophoresis-induced bonding. The normalized electric forces are estimated based on the experimental data. Future molecular dynamic simulations are demanded to determine k_i^{f0}, k_i^{r0}, Δx, and ξ.

Parameter	Definition	Figs. 6-7	Fig. 8	Fig. 9	Fig. 10	Fig. 11	Fig. 12	Fig. 13	Fig. 14	Estimation source
k_i^{f0} ($m^3 \cdot s^{-1}$)	Forward reaction rate	1×10^{-4}	1×10^{-4}	1×10^{-4}	1×10^{-4}	1×10^{-4}	1×10^{-4}	1×10^{-4}	1×10^{-4}	(Wang et al., 2017; Yu et al., 2018)
k_i^{r0} ($m^3 \cdot s^{-1}$)	Reverse reaction rate	2×10^{-6}	2×10^{-6}	2×10^{-6}	2×10^{-6}	2×10^{-6}	2×10^{-6}	2×10^{-6}	2×10^{-6}	(Wang et al., 2017; Yu et al., 2018)
Δx (m)	Distance along the energy landscape coordinate	4×10^{-9}	4×10^{-9}	4×10^{-9}	4×10^{-9}	4×10^{-9}	4×10^{-9}	4×10^{-9}	4×10^{-9}	Fitting parameter
b (m)	Kuhn segment length	5.2×10^{-10}	5.2×10^{-10}	5.2×10^{-10}	5.2×10^{-10}	5.2×10^{-10}	5.2×10^{-10}	5.2×10^{-10}	5.2×10^{-10}	(Wang et al., 2017; Wang et al., 2015; Yu et al., 2018)
n_1	Minimum chain length	10	10	10	10	10	10	10	10	Chosen based on n_a
n_m	Maximum chain length	200	200	200	300	200	200	200	200	Chosen based on n_a
n_a	Average chain length	100	100	100	50-150	100	100	100	100	Fitting parameter
δ	Chain length distribution width	0.2	0.2	0.2	0.2	0.2	0.2	0.2	0.2	(Wang et al., 2017; Wang et al., 2015; Yu et al., 2018)
ξ (N/m)	Rouse friction coefficient	4×10^{-7}	4×10^{-7}	5×10^{-8} – 1.2×10^{-6}	4×10^{-7}	4×10^{-7}	4×10^{-7}	4×10^{-7}	4×10^{-7}	Fitting parameter
H/b	Normalized boundary width	200	200	200	200	200	200	200	200	Chosen based on n_a
$E_1 qb/(k_B T)$	Normalized Electric force	0.028	0.005-0.3	0.028	0.028	0.028	0.028	0.007, 0.014, 0.028	0.028	Experimental data
$E_2 qb/(k_B T)$	Normalized Electric force for adhesion-releasing	N/A	N/A	N/A	N/A	0.028	N/A	N/A	0.007, 0.014, 0.028	Experimental data

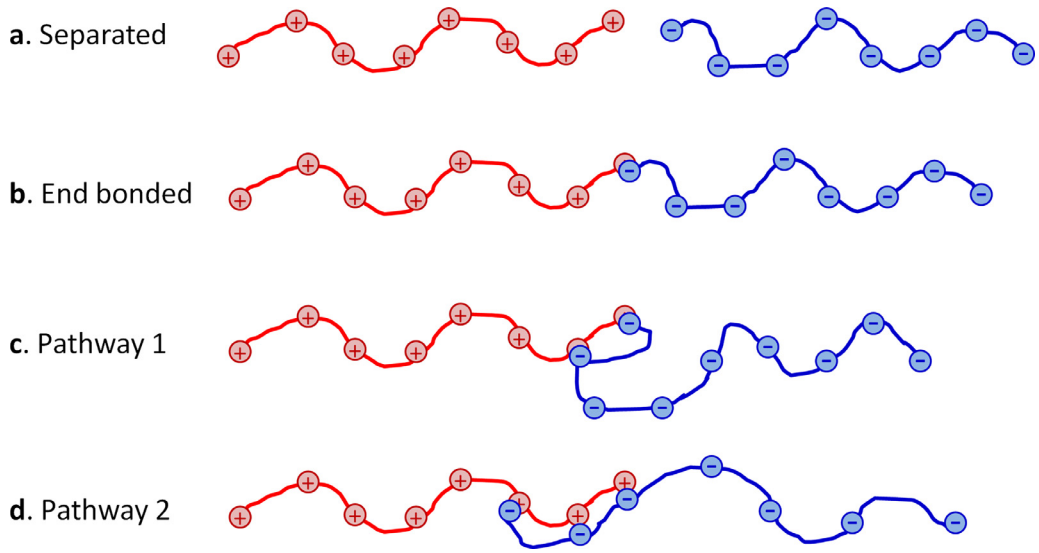

Fig. 15. (a-b) The process considered in the current model. (c) Pathway 1 and (d) pathway 2 for forming additional bonds between two charged chains.

chains at their ends. A refined model may consider forming additional bonds between two charged chains. We anticipate two possible pathways to form additional bonds (Fig. 15cd). In pathway 1, the end-bond remains unbroken and additional bonds come from the charges in the middle of the chain (Fig. 15c). This pathway violates the fundamental assumption of the reptation-like model: the chain reptates like a snake starting from the free end (De Gennes, 1979; de Gennes, 1971; Doi and Edwards, 1978; Rubinstein and Colby, 2003). Therefore, we may not consider pathway 1. In pathway 2, two chains move in parallel with the sequential bond breaking and forming (Fig. 15d). The whole theoretical framework should include Fig. 15a, b, and d. Within this framework, the increase of the interfacial strength over time is induced by not only bonding more chains but also forming more bonds within a chain. Limited by the scope of this paper, the authors have to leave this framework for the future research.

Acknowledgments

We acknowledge the funding support from the National Science Foundation (CMMI-1762567) and Air Force Office of Scientific Research Young Investigator Program (Program Manager: Dr. Jaimie S. Tiley).

Supplementary material

Supplementary material associated with this article can be found, in the online version, at doi:10.1016/j.jmps.2018.12.007.

Appendix A

We follow Slater and Noolandi to derive the statistic average of cos θ (Slater and Noolandi, 1986). We assume the ith polymer chain only moves along the curvilinear tube like a snake reptation (Fig. 5). The primitive tube length is L_C, and the chain is divided into n_i segments with each distance $\Omega = L_C/n_i$. Without the external electric field, the movement of the chain is just a snake reptation: jumping forward or backward by Ω for each step. The primitive tube length L_C is generally considered as smaller than the contour length of the ith chain $n_i b$; therefore, the step size is usually assumed as unknown. To facilitate the analysis, we here make a bold assumption that $L_C \approx n_i b$, and then

$$\Omega \approx b \tag{A1}$$

With the external electric field, the reptation is biased toward the electric field direction. Given any step vector $\mathbf{\Omega}$, we assume the vector has zero potential energy when it is perpendicular to the electric field vector $\mathbf{E}$. Then the potential energy of the step segment can be described as

$$U = -\frac{1}{2} q\mathbf{E} \cdot \mathbf{\Omega} = -\frac{1}{2} qE\Omega \cos\theta \tag{A2}$$

where θ is the angle between the electric field and the step vector ($0 \le \theta \le \pi$). The probability that a step vector has an orientation between θ and $\theta + d\theta$ is then formulated based on the potential energy as

$$G(\theta)d\theta = \Psi \frac{1}{2} \sin\theta d\theta \exp\left(-\frac{U}{k_B T}\right) = \Psi \frac{1}{2} \sin\theta d\theta \exp\left(-\frac{qE\Omega\cos\theta}{2k_B T}\right) \tag{A3}$$

where Ψ is a factor to ensure

$$\int_0^{\pi} G(\theta)d\theta = 1 \tag{A4}$$

The statistic average of $\cos\theta$ is then calculated as

$$\langle \cos\theta \rangle = \int_0^{\pi} G(\theta)\cos\theta d\theta \approx \frac{qE\Omega}{6k_BT} = \frac{qEb}{6k_BT} \tag{A5}$$

References

Acome, E., Mitchell, S., Morrissey, T., Emmett, M., Benjamin, C., King, M., Radakovitz, M., Keplinger, C., 2018. Hydraulically amplified self-healing electrostatic actuators with muscle-like performance. Science 359, 61–65.

Arruda, E.M., Boyce, M.C., 1993. A three-dimensional constitutive model for the large stretch behavior of rubber elastic materials. J. Mech. Phys. Solids 41, 389–412.

Asoh, T.-A., 2016. Electrophoretic hydrogel adhesion for fabrication of three-dimensional materials. Polym. J. 48, 1095.

Asoh, T.-A., Kawai, W., Kikuchi, A., 2012. Electrophoretic adhesion of biodegradable hydrogels through the intermediary of oppositely charged polyelectrolytes. Soft Matter 8, 1923–1927.

Asoh, T.-A., Kawamura, E., Kikuchi, A., 2013. Stabilization of electrophoretically adhered gel-interfaces to construct multi-layered hydrogels. RSC Adv. 3, 7947–7952.

Asoh, T.-A., Kikuchi, A., 2010. Electrophoretic adhesion of stimuli-responsive hydrogels. Chem. Commun. 46, 7793–7795.

Asoh, T.-A., Kikuchi, A., 2012. Rapid fabrication of reconstructible hydrogels by electrophoretic microbead adhesion. Chem. Commun. 48, 10019–10021.

Asoh, T.-A., Takaishi, K., Kikuchi, A., 2015. Adhesion of poly (vinyl alcohol) hydrogels by the electrophoretic manipulation of phenylboronic acid copolymers. J. Mater. Chem. B 3, 6740–6745.

Bell, G.I., 1978. Models for the specific adhesion of cells to cells. Science 200, 618–627.

De Gennes, P.-G., 1979. Scaling Concepts in Polymer Physics. Cornell University Press.

de Gennes, P.G., 1971. Reptation of a polymer chain in the presence of fixed obstacles. J. Chem. Phys. 55, 572–579.

Doi, M., Edwards, S.F., 1978. Dynamics of concentrated polymer systems. Part 1.-Brownian motion in the equilibrium state. J. Chem. Soc. Faraday Trans. 2 74, 1789–1801.

Ghatak, A., Chaudhury, M.K., 2003. Adhesion-induced instability patterns in thin confined elastic film. Langmuir 19, 2621–2631.

Ghatak, A., Chaudhury, M.K., Shenoy, V., Sharma, A., 2000. Meniscus instability in a thin elastic film. Phys. Rev. Lett. 85, 4329.

Graule, M., Chirarattananon, P., Fuller, S., Jafferis, N., Ma, K., Spenko, M., Kornbluh, R., Wood, R., 2016. Perching and takeoff of a robotic insect on overhangs using switchable electrostatic adhesion. Science 352, 978–982.

Grodzinsky, A., 2011. Field, Forces and Flows in Biological Systems. Garland Science.

Hänggi, P., Talkner, P., Borkovec, M., 1990. Reaction-rate theory: fifty years after Kramers. Rev. Mod. Phys. 62, 251.

He, X., Hanzon, D.W., Yu, K., 2018. Cyclic welding behavior of covalent adaptable network polymers. J. Polym. Sci. Part B Polym. Phys. 56, 402–413.

Keplinger, C., Sun, J.-Y., Foo, C.C., Rothemund, P., Whitesides, G.M., Suo, Z., 2013. Stretchable, transparent, ionic conductors. Science 341, 984–987.

Kim, C.-C., Lee, H.-H., Oh, K.H., Sun, J.-Y., 2016. Highly stretchable, transparent ionic touch panel. Science 353, 682–687.

Kim, S., Wu, J., Carlson, A., Jin, S.H., Kovalsky, A., Glass, P., Liu, Z., Ahmed, N., Elgan, S.L., Chen, W., 2010. Microstructured elastomeric surfaces with reversible adhesion and examples of their use in deterministic assembly by transfer printing. Proc. Natl. Acad. Sci. 107, 17095–17100.

Kramers, H.A., 1940. Brownian motion in a field of force and the diffusion model of chemical reactions. Physica 7, 284–304.

Larson, C., Peele, B., Li, S., Robinson, S., Totaro, M., Beccai, L., Mazzolai, B., Shepherd, R., 2016. Highly stretchable electroluminescent skin for optical signaling and tactile sensing. Science 351, 1071–1074.

Lee, Y., Cha, S.H., Kim, Y.-W., Choi, D., Sun, J.-Y., 2018. Transparent and attachable ionic communicators based on self-cleanable triboelectric nanogenerators. Nat. Commun. 9, 1804.

Li, J., Celiz, A., Yang, J., Yang, Q., Wamala, I., Whyte, W., Seo, B., Vasilyev, N., Vlassak, J., Suo, Z., 2017. Tough adhesives for diverse wet surfaces. Science 357, 378–381.

Liu, Q., Nian, G., Yang, C., Qu, S., Suo, Z., 2018. Bonding dissimilar polymer networks in various manufacturing processes. Nat. Commun. 9, 846.

Lumpkin, O.J., Déjardin, P., Zimm, B.H., 1985. Theory of gel electrophoresis of DNA. Biopolymers 24, 1573–1593.

Pu, X., Liu, M., Chen, X., Sun, J., Du, C., Zhang, Y., Zhai, J., Hu, W., Wang, Z.L., 2017. Ultrastretchable, transparent triboelectric nanogenerator as electronic skin for biomechanical energy harvesting and tactile sensing. Sci. Adv. 3, e1700015.

Ribas-Arino, J., Marx, D., 2012. Covalent mechanochemistry: theoretical concepts and computational tools with applications to molecular nanomechanics. Chem. Rev. 112, 5412–5487.

Robinson, S.S., O'Brien, K.W., Zhao, H., Peele, B.N., Larson, C.M., Mac Murray, B.C., Van Meerbeek, I.M., Dunham, S.N., Shepherd, R.F., 2015. Integrated soft sensors and elastomeric actuators for tactile machines with kinesthetic sense. Extrem. Mech. Lett. 5, 47–53.

Rubinstein, M., Colby, R., 2003. Polymer Physics. Oxford University Press, Oxford.

Sarkar, J., Sharma, A., Shenoy, V., 2005. Adhesion and debonding of soft elastic films: crack patterns, metastable pathways, and forces. Langmuir 21, 1457–1469.

Sarkar, J., Shenoy, V., Sharma, A., 2004. Patterns, forces, and metastable pathways in debonding of elastic films. Phys. Rev. Lett. 93, 018302.

Shull, K.R., Flanigan, C.M., Crosby, A.J., 2000. Fingering instabilities of confined elastic layers in tension. Phys. Rev. Lett. 84, 3057.

Slater, G.W., Noolandi, J., 1986. On the reptation theory of gel electrophoresis. Biopolymers 25, 431–454.

Sun, J.Y., Keplinger, C., Whitesides, G.M., Suo, Z., 2014. Ionic skin. Adv. Mater. 26, 7608–7614.

Treloar, L.R.G., 1975. The Physics of Rubber Elasticity. Oxford University Press.

Wang, Q., Gao, Z., Yu, K., 2017. Interfacial self-healing of nanocomposite hydrogels: theory and experiment. J. Mech. Phys. Solids 109, 288–306.

Wang, Q., Gossweiler, G.R., Craig, S.L., Zhao, X., 2015. Mechanics of mechanochemically responsive elastomers. J. Mech. Phys. Solids 82, 320–344.

Wirthl, D., Pichler, R., Drack, M., Kettlguber, G., Moser, R., Gerstmayr, R., Hartmann, F., Bradt, E., Kaltseis, R., Siket, C.M., 2017. Instant tough bonding of hydrogels for soft machines and electronics. Sci. Adv. 3, e1700053.

Yang, C.H., Chen, B., Lu, J.J., Yang, J.H., Zhou, J., Chen, Y.M., Suo, Z., 2015. Ionic cable. Extrem. Mech. Lett. 3, 59–65.

Yang, C.H., Chen, B., Zhou, J., Chen, Y.M., Suo, Z., 2016. Electroluminescence of giant stretchability. Adv. Mater. 28, 4480–4484.

Yu, K., Shi, Q., Li, H., Jabour, J., Yang, H., Dunn, M.L., Wang, T., Qi, H.J., 2016. Interfacial welding of dynamic covalent network polymers. J. Mech. Phys. Solids 94, 1–17.

Yu, K., Xin, A., Wang, Q., 2018. Mechanics of self-healing polymer networks crosslinked by dynamic bonds. J. Mech. Phys. Solids 121, 409–431.

Yuk, H., Zhang, T., Lin, S., Parada, G.A., Zhao, X., 2015. Tough bonding of hydrogels to diverse non-porous surfaces. Nat. Mater. 15, 190.

Yuk, H., Zhang, T., Parada, G.A., Liu, X., Zhao, X., 2016. Skin-inspired hydrogel–elastomer hybrids with robust interfaces and functional microstructures. Nat. Commun. 7, 12028.

Zhao, Y., Wu, Y., Wang, L., Zhang, M., Chen, X., Liu, M., Fan, J., Liu, J., Zhou, F., Wang, Z., 2017. Bio-inspired reversible underwater adhesive. Nat. Commun. 8, 2218.